

Spectral and Energy Efficiency Maximization of MISO STAR-RIS-assisted URLLC Systems

Mohammad Soleymani*, Ignacio Santamaria[†] *Senior Member, IEEE*, and Eduard Jorswieck[‡] *Fellow, IEEE*

Abstract—This paper proposes a general optimization framework to improve the spectral and energy efficiency (EE) of ultra-reliable low-latency communication (URLLC) reconfigurable intelligent surface (RIS)-assisted interference-limited systems with finite block length (FBL). This framework can be applied to any interference-limited system with treating interference as noise as the decoding strategy at receivers. Additionally, the framework can solve a large variety of optimization problems in which the objective and/or constraints are linear functions of the rates and/or EE of users. We consider a multi-cell broadcast channel as an example and show how this framework can be specialized to solve the minimum-weighted rate, weighted sum rate, global EE and weighted EE of the system. In addition to regular RIS, we consider simultaneous-transfer-and-receive (STAR)-RIS in which each passive RIS component can simultaneously reflect and transmit signals. We make realistic assumptions regarding the (STAR-)RIS by considering three different feasibility sets for the components of either regular RIS or STAR-RIS. We show that RIS can substantially increase the spectral and EE of RIS-assisted URLLC systems if the reflecting coefficients are properly optimized. Moreover, we show that STAR-RIS can outperform a regular RIS when the regular RIS cannot cover all the users.

Index Terms—Energy efficiency, finite block length, majorization minimization, MISO broadcast channels, reflecting intelligent surface, spectral efficiency, ultra-reliable low-latency communications.

I. INTRODUCTION

The sixth generation (6G) of wireless systems should be able to support many different applications such as ultra-reliable low-latency communication (URLLC), massive machine-type communication (mMTC), enhanced mobile broadband (eMBB) and internet of things (IoT) [1]–[5]. These applications typically require very low decoding error probabilities as well as very low latency and enforce us to employ a packet size much shorter than human type communications [6]. Additionally, there may exist tens of billions of various machine-type terminals such as sensors, vehicles, drones, and robots in mMTC and/or IoT networks [1], [6]. To fulfill these demands, spectral and energy efficiency (EE) should

*Mohammad Soleymani is with the Signal and System Theory Group, Universität Paderborn, Germany, <http://sst.upb.de> (email: mohammad.soleymani@sst.upb.de).

[†]Ignacio Santamaria is with the Department of Communications Engineering, University of Cantabria (email: i.santamaria@unican.es).

[‡]Eduard Jorswieck is with the Institute for Communications Technology, Technische Universität Braunschweig, 38106 Braunschweig, Germany (email: jorswieck@ifn.ing.tu-bs.de)

The work of I. Santamaria has been partly supported by the project ADELE PID2019-104958RB-C43, funded by MCIN/AEI/10.13039/501100011033.

The work of Eduard Jorswieck was supported in part by the Federal Ministry of Education and Research (BMBF, Germany) as part of the 6G Research and Innovation Cluster 6G-RIC under Grant 16KISK020K.

be drastically improved [1]. Recently, it has been shown that reconfigurable intelligent surface (RIS) can be a promising technology for enhancing the performance of various wireless networks [7]–[9].

In this work, we investigate the performance of RIS (either regular or simultaneous transmit and reflect (STAR)) in URLLC systems with finite block length (FBL) and propose a unified optimization framework to improve the spectral and EE of (STAR-)RIS-assisted URLLC systems.

A. Literature Review

Modern mobile communication systems are expected to accomplish many wide applications and services in various areas such as autonomous driving, healthcare, augmented reality, automation in industry, and so on [10]–[12]. As indicated, these application may require FBL in which the Shannon rate may not be achievable [13]. In this case, the achievable rate for a point-to-point system with Gaussian independent and identically distributed (iid) signals can be approximated as [13]

$$r = C - \alpha\sqrt{V}, \quad (1)$$

where C is the Shannon Rate, α is a constant value, which is a function of the packet length and the desired decoding error probability, and V is the channel dispersion. The rate approximation in (1) is widely known as the normal approximation (NA) [13]. The NA is known to be accurate for packet lengths more than around 124 bits and decoding error probabilities higher than 10^{-5} [14]–[17]. Note that in the third generation partnership project (3 GPP), the packet length is 32 bytes (or equivalently 256 bits), and the error probability is $\epsilon = 10^{-5}$ [5, Sec. II.D]. In general, the reliability constraint and/or packet length may vary for different services [18]. For instance, according to [18], the packet error probability should be in order of 10^{-5} for URLLC, 10^{-3} for eMBB, and 10^{-1} for mMTC. It appears that the NA should be accurate enough for these parameters if we operate in moderate or high SNR regimes [14], [15].

The performance of different systems with FBL has been studied in [19]–[24]. The authors in [19] considered the performance of non-orthogonal multiple-access (NOMA) in a multiple-access channel (MAC) with FBL. The paper [20] studied the delay performance of multiple-input, single-output (MISO) broadcast channel (BC) with imperfect channel state information (CSI) and FBL. The authors in [22] maximized the sum-rate of a single-cell MISO BC with orthogonal-frequency-division-multiple-access (OFDMA)-URLLC. The paper [23] maximized the minimum rate of a MISO URLLC BC. The

authors in [24] studied a massive multiple-input, multiple-output (MIMO) URLLC with FBL and proposed schemes to maximize the minimum rate and EE of the network.

To be able to support URLLC, one of the targets of 6G is to improve the spectral and EE [1]. Energy efficient techniques are very important for IoT and/or industrial IoT (IIoT) and/or MTC since such techniques can increase the battery life of devices and reduce the implementation and/or maintenance expenses [1], [11]. To improve spectral and EE, 6G will employ some emerging technologies such as RIS, which can enhance the coverage and consequently, the system performance [7]–[9], [25]. RIS has been employed to improve the performance of various systems with realistic assumptions regarding the CSI and devices [26]–[36]. For instance, the papers [31], [34] considered a multi-cell MIMO RIS-assisted BC and showed that RIS can improve the spectral and EE of the system. The superiority of RIS in a single-cell MISO BC was shown in [28]–[30]. The papers [33], [35] applied NOMA to multi-cell RIS-assisted BCs and showed that NOMA can enhance the system performance. The authors in [27] showed that RIS can improve the performance of an OFDM system. We refer the reader to [7], [9] for an overview of RIS.

A regular RIS can only reflect signals, which may restrict the coverage area of the RIS. For a 360° coverage, a STAR-RIS has been proposed in which each passive element can reflect and transmit at the same time [37]–[44]. STAR-RIS is a novel technology and has been evaluated by experimental results [45]. Due to a wider coverage area by STAR-RIS, it can be expected that STAR-RIS is able to support more applications especially when it is not possible to locate a regular RIS such that all transceivers are in its reflection area.

All the aforementioned papers on RIS, [7]–[9], [25]–[36], considered the performance of RIS in systems with infinite block length. The performance of RIS in the presence of FBL has been studied in [46]–[56]. The paper [46] studied the performance of RIS and unmanned aerial vehicles (UAVs) in URLLC systems and showed that RIS can be beneficial in the system. The authors in [47] considered NOMA in RIS-assisted single-input, single-output (SISO) BC with two users and showed that RIS can improve the system throughput and decrease the average decoding error rate. The performance of RIS in MISO point-to-point URLLC systems with a factory automation scenario was investigated in [48], where the average data rate and decoding error probability were obtained under different assumptions regarding the fading and propagation of the channels. The authors in [49] minimized the latency of a single-cell SISO RIS-assisted URLLC BC with user grouping. The paper [50] considered RIS-assisted URLLC systems with FBL to transfer information and energy wirelessly. The paper [51] proposed resource allocation schemes for RIS-assisted single-cell BCs with the coexistence of eMBB and URLLC services.

It is worth emphasizing that the optimal channel dispersion in (1) is

$$V^{opt} = 1 - \frac{1}{(1 + \gamma)^2}, \quad (2)$$

where γ is the SNR. Even if we treat interference as noise, we cannot simply replace the SNR term by signal-to-interference

plus-noise ratio (SINR) and use the same channel dispersion for interference-limited systems [57]. Indeed the optimal channel dispersion cannot be achieved by Gaussian signals in the presence of interference. Unfortunately, this issue is sometimes overlooked in the literature when studying an interference-limited system. In this paper, we consider the channel dispersion in [57], which can be achieved by Gaussian signals in interference-limited systems with treating interference as noise (TIN). To the best of our knowledge, [56] is the only work in interference-limited RIS-assisted systems with FBL that considered the channel dispersion in [57]. Note that [56] studied the geometric mean of the rates. However, in this paper, we consider various utility functions as will be discussed in the next subsection.

B. Motivations and contributions

The main motivation for this work is to propose a general framework for URLLC RIS-assisted systems. In Table I, we provide a brief summary of the most related works based on the considered scenario and the channel dispersion. As can be observed, even though RIS has received many attentions during recent years, the performance of RIS in URLLC with FBL should be further investigated, especially in multi-user communication systems. For instance, to the best of our knowledge, there is no work on STAR-RIS in URLLC with FBL. Additionally, EE metrics have not been considered in RIS-assisted URLLC systems with FBL. It should be emphasized that the rate expressions with FBL are more complicated than the Shannon rates, and it is not straightforward to modify and apply existing optimization approaches to URLLC RIS-assisted systems with FBL. Thus, a unified optimization framework is required to study the performance of such systems by considering STAR-RIS and EE metrics.

In this paper, we propose a general optimization framework for URLLC with FBL in RIS-assisted systems. This framework can be applied to any optimization problem in which the objective and/or the constraints are linear functions of the rates and/or EE of users. Moreover, the framework can be applied to any interference-limited system with treating interference as noise (TIN). This framework is based on majorization minimization (MM) and alternating optimization (AO). MM is an iterative algorithm, which converges to a stationary point of the considered optimization problem [58]. In the proposed framework, we first optimize over the beamforming vectors for given RIS components. We then alternate and optimize the RIS components for given beamforming vectors.

We consider a multi-cell MISO RIS-assisted BC as an illustrative example and show how the unified framework can be specialized to solve different optimization problems. To this end, we consider the minimum-weighted-rate, weighted-sum-rate, global EE and minimum-weighted-EE maximization problems. We also make realistic assumptions regarding RIS (either regular or STAR) by modeling the small-scale and large-scale fading and considering three different feasibility sets based on the models in [7], [38]–[41]. We propose three main approaches to optimize reflecting/transmitting coefficients in STAR-RIS. First, we assume that a set of RIS

TABLE I: A brief comparison of the most related works.

	RIS	STAR-RIS	URLLC	Multi-user communications	Multiple-antenna Systems	Channel dispersion in [57]	EE metrics
This paper	✓	✓	✓	✓	✓	✓	✓
[22], [23]			✓	✓	✓		
[19]			✓	✓		✓	
[20]			✓	✓	✓	✓	
[24]			✓	✓	✓	✓	✓
[29]–[32]	✓			✓	✓		
[28], [34], [35]	✓			✓	✓		✓
[36]	✓	✓		✓	✓		✓
[46], [55]	✓		✓	✓	✓		
[47], [49], [51]	✓		✓	✓			
[48], [50]	✓		✓		✓		
[56]	✓		✓	✓		✓	

components operate only in the reflection mode, and the remaining components operate only in the transmission mode. This scheme is referred to as the mode switching [37]. Second, we assume that all the components simultaneously operate in both reflection and transmission mode, which is referred to as the energy splitting mode [37]. Third, we assume that each time slot is divided into two sub-slots. Then, all the components operate in the reflection mode in the first sub-slot, while they all operate in the transmission mode in the next sub-slot. This scheme is referred to as time switching [37].

Through numerical examples, we show that RIS can significantly improve the spectral or the energy efficiency of the system when the reflecting coefficients are properly optimized. Interestingly, it may happen in some special cases that RIS worsen the performance if the reflecting coefficients are chosen randomly. Additionally, we show that STAR-RIS with mode switching and energy splitting approaches outperforms regular RIS when the RIS cannot cover all the users. The mode-switching scheme of STAR-RIS slightly improves the system performance over regular RIS. However, the energy-splitting scheme considerably outperforms the regular RIS.

The main contributions of this work can be summarized as follows:

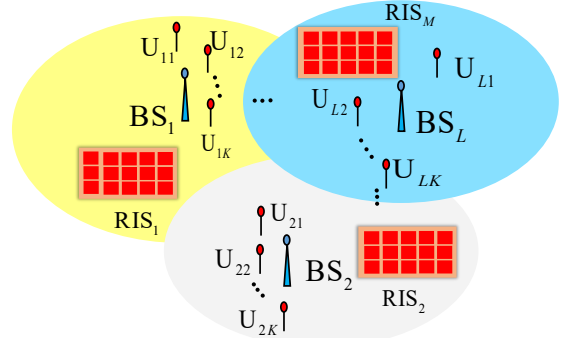
- We propose a unified optimization framework to solve a large family of optimization problems for MISO STAR-RIS-assisted interference-limited URLLC systems. This framework can be applied to any interference-limited system with TIN.
- We consider a multicell BC and specialize the framework to solve minimum-weighted rate, weighted-sum rate, minimum-weighted rate, and global EE maximization problems.
- We study the performance of STAR-RIS with three different feasibility sets and consider three schemes for optimizing the reflecting/transmitting coefficients of STAR-RIS. We show that STAR-RIS may outperform regular RIS if the regular RIS cannot cover all the users.
- We show that RIS can substantially improve the spectral and EE of RIS-assisted URLLC systems by considering different utility functions and feasibility sets for RIS components.

C. Paper outline

The rest of the paper is organized as follows. Section II presents the system model and formulate the considered

TABLE II: List of frequently used notations.

L/M	No. of BSs/RISs
K	No. of users per each cell
N_{BS}/N_{RIS}	No. of antennas/components at each BS/RIS
u_{lk}	k -th associated user to BS l
s_{lk}	Transmit signal of BS l intended for u_{lk}
\mathbf{x}_{lk}	Beamforming vector of BS l corresponding to s_{lk}
$\mathbf{h}_{lk,i}$	Equivalent channel between BS i and u_{lk}
$\mathbf{d}_{jk,l}$	Direct channel between the BS l and u_{jk}
$\mathbf{f}_{jk,m}$	Channel between the m th RIS and u_{jk}
\mathbf{G}_{ml}	Channel between the BS l and the m th RIS
Θ_m	Matrix of RIS components for the m th RIS
ϵ^c	Decoding error probability
n_{lk}	Additive white Gaussian noise at u_{lk}
e_{lk}/r_{lk}	Energy efficiency/rate of u_{lk}
V_{lk}	Channel dispersion at u_{lk}
p_l	Power budget of BS l
γ_{lk}	SINR at u_{lk}
n_t	Packet length

**Fig. 1:** A multicell broadcast channel with RIS.

problem. Section III presents the generalized optimization framework for the systems without RIS. Section IV states the extension of the proposed optimization framework to URLLC (STAR-)RIS-assisted systems. Section V provides some numerical results. Section VI concludes the paper. Finally, we provide some proofs in appendices.

II. SYSTEM MODEL

Our unified optimization framework can be applied to a large class of interference-free and/or interference-limited URLLC MISO (STAR)-RIS-assisted systems with TIN. Such systems include, for instance, various multi-user interference channels, cognitive radio systems, broadcast channels, multiple-access channels, device-to-device communications, and so on. For the sake of illustration, we consider a multicell broadcast channel with L multi-antenna base stations (BSs)

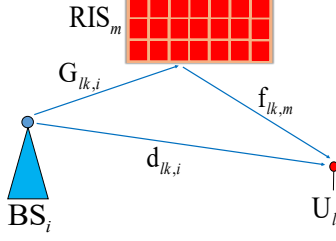


Fig. 2: Channel model in a typical RIS-assisted system.

in which each BS has N_{BS} antennas and serves K single-antenna users. We assume that there are $M \geq L$ RISs with N_{RIS} reflecting elements in the system to assist the BSs. Note that a multicell BC is a practical scenario, which is considered in many work such as [31], [33], [36], [43]. In a multicell BC, intercell interference may highly degrade the system performance especially for cell-edge users, which should be handled by a joint optimization of transmit parameters at BSs.

We assume perfect, global and instantaneous channel state information (CSI) at all transceivers similar to many other works on RIS (either STAR or regular) such as [26], [28]–[33], [41], [59]–[63]. Investigating the performance of RIS with perfect CSI can show the main tradeoffs in the system design and provide an upper bound for the system performance. Indeed, studying the performance of RIS with perfect CSI can show whether/how (STAR-)RIS can provide any benefit in URLLC systems. If the benefits of RIS are minor with perfect CSI, then it may imply that RIS cannot be beneficial in more realistic scenarios. We also assume that BSs use short-length packets to transmit data to the users. Without loss of generality, we consider a symmetric scenario with the same number of BS antennas or users per cell. However, our work can be easily extended to an asymmetric scenario in which each BS has a different number of antennas/associated users.

A. RIS model

In this paper, we consider both regular and STAR-RISs. Here, we briefly describe the model here and refer the readers to [31], [34], [7, Sec. II] or [41] for a detailed description/review on the features of RIS and/or STAR-RIS.

1) *Regular RIS*: As shown in Fig. 2, the channel between BS i and user k associated to BS l , i.e., \mathbf{u}_{lk} , is

$$\mathbf{h}_{lk,i}(\{\Theta\}) = \underbrace{\sum_{m=1}^M \mathbf{f}_{lk,m} \Theta_m \mathbf{G}_{mi}}_{\text{Links through RIS}} + \underbrace{\mathbf{d}_{lk,i}}_{\text{Direct link}} \in \mathbb{C}^{1 \times N_{BS}}, \quad (3)$$

where $\mathbf{d}_{lk,i}$ is the direct link between BS i and \mathbf{u}_{lk} , \mathbf{G}_{mi} is the channel matrix between BS i and RIS m , $\mathbf{f}_{lk,m}$ is the channel vector between RIS m and \mathbf{u}_{lk} , and Θ_m is

$$\Theta_m = \text{diag}(\theta_{m1}, \theta_{m2}, \dots, \theta_{mN_{RIS}}), \quad (4)$$

where θ_{mi} s for all m, i are the reflecting coefficients. Hereafter, we drop the dependency of the channels with respect to $\{\Theta\}$ for notational simplicity.

The channels can be optimized only through the reflecting coefficients θ_{mi} , which are complex-valued parameters. There

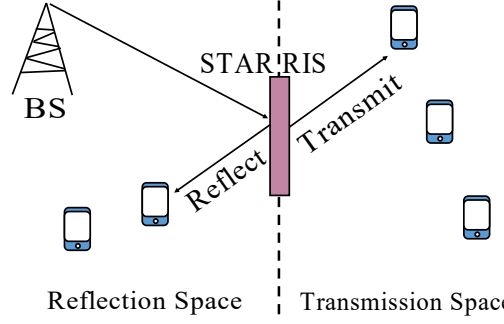


Fig. 3: A typical STAR-RIS-assisted system.

are different assumptions for modeling the reflecting coefficients. In this paper, we consider three different feasibility sets for θ_{mi} s based on the models in [7, Sec. II]. An upper bound for RIS performance can be achieved by considering the amplitude and phase of θ_{mi} s as independent random variables, which results in the following feasibility set [7, Eq. (11)]

$$\mathcal{T}_U = \{\theta_{mn} : |\theta_{mn}|^2 \leq 1 \ \forall m, n\}. \quad (5)$$

A more common feasibility set is

$$\mathcal{T}_I = \{\theta_{mi} : |\theta_{mi}| = 1 \ \forall m, i\}, \quad (6)$$

which has been widely used in the literature [7], [9], [26], [29]–[32]. Another practical feasibility set is [64]

$$\mathcal{T}_C = \{\theta_{mi} : |\theta_{mi}| = \mathcal{F}(\angle \theta_{mi}), \angle \theta_{mi} \in [-\pi, \pi] \ \forall m, i\}. \quad (7)$$

In this model, the amplitude of each RIS element is a deterministic function of its phase as [64]

$$\mathcal{F}(\angle \theta_{mi}) = |\theta|_{\min} + (1 - |\theta|_{\min}) \left(\frac{\sin(\angle \theta_{mi} - \phi) + 1}{2} \right)^\alpha, \quad (8)$$

where $|\theta|_{\min}$, α , and ϕ are non-negative constant values.

2) *STAR-RIS*: In a regular RIS, each RIS component can only reflect the signals. However, STAR-RIS allows each component to not only reflect, but also transmit signals simultaneously, as its name suggests. Thus, a STAR-RIS can cover a larger area as shown in Fig. 3. Indeed, there are two spaces for each RIS: reflection space (RS) and transmission space (TS), while a regular RIS can only reflect [37].

In STAR-RIS-assisted systems, each user belongs to either RS or TS [37]. We represent the reflecting and transmit coefficients of the i -th component of the m -th RIS by, respectively, θ_{mi}^r and θ_{mi}^t . In case of STAR-RIS, the channel between BS i and \mathbf{u}_{lk} is [37, Eq. (2)]

$$\mathbf{h}_{lk,i} = \underbrace{\sum_{m=1}^M \mathbf{f}_{lk,m} \Theta_m^{r/t} \mathbf{G}_{mi}}_{\text{Links through RIS}} + \underbrace{\mathbf{d}_{lk,i}}_{\text{Direct link}},$$

where $\Theta_m^r = \text{diag}(\theta_{m1}^r, \theta_{m2}^r, \dots, \theta_{mN_{RIS}}^r)$, and $\Theta_m^t = \text{diag}(\theta_{m1}^t, \theta_{m2}^t, \dots, \theta_{mN_{RIS}}^t)$. The upper bound for the performance of STAR-RIS is given by the following feasibility set [40, Eq. (2)]

$$\mathcal{T}_{SU} = \{\theta_{mn}^r, \theta_{mn}^t : |\theta_{mn}^r|^2 + |\theta_{mn}^t|^2 \leq 1 \ \forall m, n\}. \quad (9)$$

A more common feasibility set is [38], [39, Eq. (1)]

$$\mathcal{T}_{SI} = \{\theta_{mn}^r, \theta_{mn}^t : |\theta_{m_i}^r|^2 + |\theta_{m_i}^t|^2 = 1 \ \forall m, i\}. \quad (10)$$

In these feasibility sets, the phases of the reflection and transmission coefficients can be independently optimized. However, another feasibility set has been studied in [41], [63] in which the phases completely depend on each other. This feasibility set can be written as [41, Proposition 1]

$$\mathcal{T}_{SN} = \{\theta_{mn}^r, \theta_{mn}^t : |\theta_{m_i}^r|^2 + |\theta_{m_i}^t|^2 = 1, \Re\{\theta_{m_i}^{r*} \theta_{m_i}^t\} = 0 \ \forall m, i\}. \quad (11)$$

Lemma 1. *The two constraints $|\theta_{m_i}^r|^2 + |\theta_{m_i}^t|^2 = 1$ and $\Re\{\theta_{m_i}^{r*} \theta_{m_i}^t\} = 0$ are equivalent to the following constraints:*

$$|\theta_{m_i}^r + \theta_{m_i}^t|^2 \leq 1, \quad (12)$$

$$|\theta_{m_i}^r - \theta_{m_i}^t|^2 \leq 1, \quad (13)$$

$$|\theta_{m_i}^r|^2 + |\theta_{m_i}^t|^2 = 1. \quad (14)$$

Proof. We have the following equality

$$|\theta_{m_i}^r \pm \theta_{m_i}^t|^2 = |\theta_{m_i}^r|^2 + |\theta_{m_i}^t|^2 \pm 2\Re\{\theta_{m_i}^{r*} \theta_{m_i}^t\}. \quad (15)$$

Substituting $|\theta_{m_i}^r|^2 + |\theta_{m_i}^t|^2$ by 1, the constraints (12) and (13) simplify to $\pm\Re\{\theta_{m_i}^{r*} \theta_{m_i}^t\} \leq 0$, which is equivalent to $\Re\{\theta_{m_i}^{r*} \theta_{m_i}^t\} = 0$. \square

B. Signal model

The broadcast signal from BS l is

$$\mathbf{x}_l = \sum_{k=1}^K \mathbf{x}_{lk} s_{lk} \in \mathbb{C}^{N_{BS} \times 1}, \quad (16)$$

where $s_{lk} \sim \mathcal{CN}(0, 1)$ is the message intended for the k -th user associated to the l -th BS, denoted by \mathbf{u}_{lk} , and \mathbf{x}_{lk} is the corresponding beamforming vectors, which is an optimization parameter. Note that s_{lk} s for all l, k are independent and identically distributed (iid) proper Gaussian signals.

The received signal for the user \mathbf{u}_{lk} is

$$y_{lk} = \sum_{i=1}^L \mathbf{h}_{lk,i} \sum_{j=1}^K \mathbf{x}_{ij} s_{ij} + n_{lk} \quad (17a)$$

$$= \underbrace{\mathbf{h}_{lk,l} \mathbf{x}_{lk} s_{lk}}_{\text{Desired signal}} + \underbrace{\mathbf{h}_{lk,l} \sum_{j=1, j \neq k}^K \mathbf{x}_{lj} s_{lj}}_{\text{Intracell interference}} + \underbrace{\sum_{i=1, i \neq l}^L \mathbf{h}_{lk,i} \mathbf{x}_i}_{\text{Intercell interference}} + \underbrace{n_{lk}}_{\text{Noise}} \quad (17b)$$

where $\mathbf{h}_{lk,l} \in \mathbb{C}^{1 \times N_{BS}}$ is the channel between BS l and \mathbf{u}_{lk} , and $n_{lk} \sim \mathcal{CN}(0, \sigma^2)$ is additive white Gaussian noise. As can be easily verified through (17), the received signal and the interference term are proper Gaussian signals. Furthermore, the noise, interference and desired signals are independent from each other.

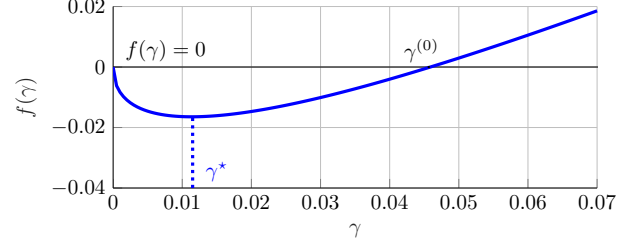


Fig. 4: $f(\gamma)$ versus γ for $a = 0.2185$. It represents $r_{l,k} / \ln 2$ as a function of $\gamma_{l,k}$ for $n_t = 200$, and $\epsilon = 10^{-3}$.

C. Rate and energy efficiency expressions

Each user decodes its own message, treating all other signals as noise. Thus, the rate of \mathbf{u}_{lk} is [13], [24, Eq. (8)]

$$r_{lk} = \underbrace{\log_2(1 + \gamma_{lk})}_{\text{Shannon Rate}} - \underbrace{Q^{-1}(\epsilon^c) \sqrt{\frac{V_{lk}}{n_t}}}_{\delta_{lk}(\{\mathbf{x}\}, \{\Theta\})}, \quad (18)$$

where V_{lk} is the channel dispersion for decoding s_{lk} at \mathbf{u}_{lk} , n_t is the packet length, Q^{-1} is the inverse of the Gaussian Q-function, ϵ^c is an acceptable decoding error probability, which indicates that one out of $1/\epsilon^c$ short-length packets may experience outage, and γ_{lk} is the corresponding SINR given by

$$\gamma_{lk} = \frac{|\mathbf{h}_{lk,l} \mathbf{x}_{lk}|^2}{\sigma^2 + \sum_{ij \neq lk} |\mathbf{h}_{lk,i} \mathbf{x}_{ij}|^2}, \quad (19)$$

where $\sum_{[ij] \neq [lk]} |\mathbf{h}_{lk,i} \mathbf{x}_{ij}|^2 = \sum_{ij} |\mathbf{h}_{lk,i} \mathbf{x}_{ij}|^2 - |\mathbf{h}_{lk,l} \mathbf{x}_{lk}|^2$. We represent the gap between the Shannon rate and the FBL by $\delta_{lk}(\{\mathbf{x}\}, \{\Theta\}, \epsilon^c) = Q^{-1}(\epsilon^c) \sqrt{V_{lk}/n_t}$, which is a function of the channel dispersion. Note that ϵ^c is related to the reliability constraint, and the gap between the Shannon rate and the FBL increases with the reliability. In other words, to ensure a more reliable communication (lower ϵ^c), we should transmit data at a rate lower than the Shannon rate. The optimal channel dispersion is [13]

$$V_{lk}^{opt} = 1 - \frac{1}{(1 + \gamma_{lk})^2} = \frac{\gamma_{lk}}{1 + \gamma_{lk}} \left(1 + \frac{1}{1 + \gamma_{lk}} \right). \quad (20)$$

However, it is not achievable by iid Gaussian signals when there exists interference. In [57], the authors proposed a simple and practical scheme, which is not dispersion optimal. The channel dispersion for the scheme in [57] is

$$V_{lk} = 2 \frac{\gamma_{lk}}{1 + \gamma_{lk}} = 2 \left(1 - \frac{1}{1 + \gamma_{lk}} \right). \quad (21)$$

Note that it can be easily verified that the dispersion in (21) is an upper bound for (20). Additionally, it should be noted that the FBL rate, Shannon rate, channel dispersion and δ are a function of ϵ^c , $\{\mathbf{x}\}$ and $\{\Theta\}$. However, due to a notational simplicity, we drop this dependency in the equations unless it causes confusion. In the following lemma, we take a look at the structure of (18), which provides an insight for optimizing over the FBL rates by the NA.

Lemma 2. *Consider the function*

$$f(\gamma) = \ln(1 + \gamma) - a \sqrt{\frac{\gamma}{1 + \gamma}},$$

where $\gamma \geq 0$ is a variable, and $a > 0$ is a given and constant parameter. Then, $f(\gamma)$ is minimized at γ^* , where $f(\gamma^*) < 0$. Moreover, $f(\gamma)$ is strictly decreasing in $0 \leq \gamma < \gamma^*$, and strictly increasing for $\gamma > \gamma^*$ (see Fig. 4). Additionally, $f(\gamma)$ has two root given by $\gamma = 0$, and $\gamma = \gamma^{(0)}$.

Proof. The derivative of $f(\gamma)$ with respect to γ is

$$\frac{\partial f}{\partial \gamma} = \frac{1}{1+\gamma} - \frac{a}{2} \left(\frac{\gamma}{1+\gamma} \right)^{-\frac{1}{2}} \left(\frac{1}{1+\gamma} \right)^2,$$

which can be simplified as $\frac{\partial f}{\partial \gamma} = \frac{1}{1+\gamma} \left[1 - \frac{a}{2} \frac{1}{\sqrt{\gamma(1+\gamma)}} \right]$. The function $\frac{1}{\sqrt{\gamma(1+\gamma)}}$ is strictly decreasing in γ and takes values ∞ for $\gamma = 0$ and 0 for $\gamma = \infty$, which proves the lemma. \square

The achievable rate with FBL in (18) is a difference of two terms, which are functions of γ_{lk} . It should be emphasized that the expression in (18) is indeed an approximation for the actual achievable rate and may not be accurate in very low SINR regimes and/or for a very short packet length and/or low decoding error probability [14]–[17], [65]. According to Lemma 2, r_{lk} can be negative for very low γ_{lk} (see Fig. 4), which implies that (18) is not an accurate approximation for $\gamma_{lk} \ll 1$, which is also confirmed by the results in [65]. We refer the reader to [13, Sec. IV.C] for detailed discussions on the accuracy of the NA with different parameters.

The energy efficiency (EE) of a user is defined as the ratio between its data rate and the power consumption for transmitting the data as [66]

$$e_{lk} = \frac{r_{lk}}{p_c + \eta \mathbf{x}_{lk}^H \mathbf{x}_{lk}}, \quad (22)$$

where η^{-1} is the power efficiency of each BS, and p_c is the constant power consumption in the network for transmitting data to a user, which is given by [34, Eq. (27)]. Another metric for EE is the global EE (GEE), which considers the performance of the whole network. The GEE is defined as ratio between the total achievable rate and the total power consumption of the network, i.e., [66]

$$GEE = \frac{\sum_{lk} r_{lk}}{LKp_c + \eta \sum_{lk} \mathbf{x}_{lk}^H \mathbf{x}_{lk}}. \quad (23)$$

D. Problem statement

We consider a general optimization problem, which includes a large variety of optimization problems. This general optimization problem can be formulated as

$$\max_{\{\mathbf{x}\} \in \mathcal{X}, \{\Theta\} \in \mathcal{T}} f_0(\{\mathbf{x}\}, \{\Theta\}) \text{ s.t. } f_i(\{\mathbf{x}\}, \{\Theta\}) \geq 0, \forall i, \quad (24a)$$

$$r_{lk} \geq r^{th}, \quad \forall l, k, \quad (24b)$$

where \mathcal{X} and \mathcal{T} are, respectively, the feasibility sets for $\{\mathbf{x}\}$ and $\{\Theta\}$. The feasibility set \mathcal{X} is

$$\mathcal{X} = \left\{ \{\mathbf{x}\} : \sum_{lk} \mathbf{x}_{lk}^H \mathbf{x}_{lk} \leq p_l, \forall l, k \right\}, \quad (25)$$

where p_l is the power budget for BS l . The constraint (24b) is related to the latency constraint of the system. If the

maximum tolerable latency is t_c seconds, then the minimum achievable rate of each user per bandwidth unit should be greater than $r^{th} = \frac{n_t}{t_c w}$, where w is the channel bandwidth in Hz, and n_t is the packet length in bits. Moreover, f_i for all i are linear functions of rates/EEs. Note that f_i can also include some other linear/quadratic/convex/concave constraints in beamforming vectors/channels such as an energy harvesting constraint and/or the so-called interference temperature. However, due to a space restriction, we do not consider such constraints in this work and leave them for a future study.

In this paper, we aim at proposing a unified optimization framework to solve the general optimization problem (24), which includes, for example, maximization of weighted-sum rate, maximization of minimum-weighted rates, global EE, and maximization of the minimum-weighted EE. Note that it could be possible to focus on a specific optimization problem and provide a detailed solution for it with different approaches, each with a different behavior in terms of complexity and optimality. However, it is also very important to concentrate on a general methodology for solving various problems with different utility/cost functions. In this work, we prefer to choose the second approach especially since the performance of RIS (either regular or STAR) should be further investigated in FBL regimes, and a general optimization framework can provide an effective tool to do so.

III. GENERALIZED OPTIMIZATION FRAMEWORK FOR SYSTEMS WITHOUT RIS

In this section, we consider the optimization of the beamforming vectors $\{\mathbf{x}\}$ for systems without RIS. Note that the algorithms in this section can be applied to RIS-assisted systems when the reflecting coefficients are fixed. The considered optimization problem in this section is

$$\max_{\{\mathbf{x}\} \in \mathcal{X}} f_0(\{\mathbf{x}\}) \quad \text{s.t. } f_i(\{\mathbf{x}\}) \geq 0, \forall i, \quad (26a)$$

$$r_{lk} \geq r^{th}, \quad \forall l, k, \quad (26b)$$

Unfortunately, (26) is not convex since the rates are not concave in $\{\mathbf{x}\}$. To solve (26), we employ MM, which is an iterative algorithm and consists of two steps in each iteration: majorization and minimization [58]. In the majorization step, the non-convex constraints (and/or objective function) are approximated by suitable surrogate functions. Note that the surrogate functions in MM algorithms should fulfill three specific conditions mentioned in, e.g., [67, Sec. III]. In the minimization step, the corresponding surrogate optimization problem is solved. It should be noted that MM is a powerful and standard optimization technique. MM encompasses many well-known optimization techniques such as expectation maximization (EM), successive convex approximation (SCA), difference of convex programming (DCP), convex-concave procedure (CCP), cyclic minimization, proximal minimization, some fractional programming techniques, and so on [58]. Moreover, MM has many applications not only in communications, but also in machine learning, signal processing, and other research areas [58]. One of the most challenging parts in MM is to find suitable surrogate functions such that the corresponding optimization problem can be efficiently solved.

In communication systems, we mostly deal with rate functions, which are usually continuous and differentiable in the domain of the optimization parameters such as powers, beamforming vectors, and channels. Additionally, the Shannon rates are in a logarithmic format. Thus, we can employ the CCP to obtain suitable surrogate functions for rates and/or EE functions (please refer to [36, Appendix B] for some examples).

Note that MM starts with a feasible initial point and converges to a stationary point of the considered optimization problem, which meets the first order optimality constraint and satisfies the Karush-Kuhn-Tucker (KKT) conditions [68]. Since we employ MM, our proposed framework for systems without RIS converges to a stationary point of (26). The final point of MM-based algorithms may depend on the initial point, which should be feasible and can be chosen either randomly or heuristically [69]. As indicated in Section II-C, the rates in (18) may not be accurate for very low SINR, i.e., $\gamma_{lk} \ll 1$. Additionally, the latency constraint in (26b) may not be satisfied for a random initial point. Thus, to obtain a feasible and suitable initial point, we can employ the approach in Appendix A, which takes the solution of the maximization of the minimum SINR of users as an initial point.

In the proposed framework, we firstly approximate the rates by suitable concave lower-bound surrogate functions and then, solve the corresponding surrogate optimization problem. To this end, we employ the lower-bounds in the following lemma.

Lemma 3. A concave lower bound for r_{lk} is

$$r_{lk} \geq \tilde{r}_{lk} = a_{lk} + \frac{2\Re\left\{\left(\mathbf{h}_{lk,l}\mathbf{x}_{lk}^{(t-1)}\right)^*\mathbf{h}_{lk,l}\mathbf{x}_{lk}\right\}}{\sigma^2 + \sum_{[ij] \neq [lk]} \left|\mathbf{h}_{lk,i}\mathbf{x}_{ij}^{(t-1)}\right|^2} + \frac{2Q^{-1}(\epsilon^c)}{\sqrt{n_t V_{lk}^{(t-1)}}} \frac{\sigma^2 + \sum_{[ij] \neq [lk]} \Re\left\{\left(\mathbf{h}_{lk,i}\mathbf{x}_{ij}^{(t-1)}\right)^*\mathbf{h}_{lk,i}\mathbf{x}_{ij}\right\}}{\sigma^2 + \sum_{ij} \left|\mathbf{h}_{lk,i}\mathbf{x}_{ij}^{(t-1)}\right|^2} - b_{lk} \frac{\sigma^2 + \sum_{ij} \left|\mathbf{h}_{lk,i}\mathbf{x}_{ij}^{(t-1)}\right|^2}{\sigma^2 + \sum_{ij} \left|\mathbf{h}_{lk,i}\mathbf{x}_{ij}^{(t-1)}\right|^2}, \quad (27)$$

where t is the number of the current iteration, a_{lk} , and b_{lk} are constants and, respectively, give by

$$a_{lk} = \log_2 \left(1 + \gamma_{lk}^{(t-1)}\right) - \gamma_{lk}^{(t-1)} - \frac{Q^{-1}(\epsilon^c)}{\sqrt{n_t}} \left(\frac{\sqrt{V_{lk}^{(t-1)}}}{2} + \frac{1}{\sqrt{V_{lk}^{(t-1)}}}\right),$$

$$b_{lk} = \gamma_{lk}^{(t)} + \frac{\zeta_{lk}^{(t-1)} Q^{-1}(\epsilon^c)}{\sqrt{n_t V_{lk}^{(t-1)}}},$$

where $\gamma_{lk}^{(t-1)}$ and $V_{lk}^{(t-1)}$ are, respectively, obtained by replacing $\{\mathbf{x}^{(t-1)}\}$ in (19) and (21). Moreover,

$$\zeta_{lk}^{(t-1)} = \frac{\sigma^2 + \sum_{[ij] \neq [lk]} \left|\mathbf{h}_{lk,i}\mathbf{x}_{ij}^{(t-1)}\right|^2}{\sigma^2 + \sum_{ij} \left|\mathbf{h}_{lk,i}\mathbf{x}_{ij}^{(t-1)}\right|^2}.$$

The concave lower bound in (27) is quadratic in $\{\mathbf{x}\}$, and is obtained by deriving a concave lower bound for the Shannon rate as well as by finding a convex upper bound for δ_{lk} .

Proof. Please refer to Appendix C. \square

Note that the concave lower-bound rates \tilde{r}_{lk} for all l, k are quadratic in \mathbf{x}_{ij} for all i, j . Substituting \tilde{r}_{lk} s in f_i s gives the surrogate functions \tilde{f}_i s and consequently, the following surrogate optimization problem

$$\max_{\{\mathbf{x}\} \in \mathcal{X}} \tilde{f}_0(\{\mathbf{x}\}) \quad \text{s.t. } \tilde{f}_i(\{\mathbf{x}\}) \geq 0, \quad \forall i, \quad (28a)$$

$$\tilde{r}_{lk} \geq r_{lk}^{th}, \quad \forall l, k. \quad (28b)$$

This optimization problem is convex for spectral efficiency metrics, which can be efficiently solved by numerical tools. However, (28) is not convex if we consider EE metrics. In this case, we can obtain the global optimal solution of (28) by Dinkelbach-based algorithms [66]. Note that the proposed framework converges to a stationary point of (24) since it falls into MM. In the following subsections, we will discuss the solutions of (28) with different utility functions. To this end, we select the minimum-weighted rate, weighted-sum rate, global EE, and minimum-weighted EE as utility functions since they are among the most important metrics in practice as well as in the literature either with Shannon rate or in FBL regimes [22]–[24], [36], [70]–[73].

A. Minimum-weighted rate maximization

The maximization of the minimum-weighted rate can be written as

$$\max_{\{\mathbf{x}\} \in \mathcal{X}, r} r \quad \text{s.t. } r_{lk} \geq \max(\lambda_{lk} r, r^{th}) \quad \forall l, k, \quad (29)$$

where λ_{lk} s are the weights corresponding to the priorities assigned to the users. Employing the lower bounds in Lemma (3), we have the following surrogate optimization problem

$$\max_{\{\mathbf{x}\} \in \mathcal{X}, r} r \quad \text{s.t. } \tilde{r}_{lk} \geq \max(\lambda_{lk} r, r^{th}) \quad \forall l, k, \quad (30)$$

which is convex and can be efficiently solved.

B. Weighted-sum rate maximization

The weighted-sum-rate maximization problem is

$$\max_{\{\mathbf{x}\} \in \mathcal{X}} \sum_{lk} \lambda_{lk} r_{lk} \quad \text{s.t. } r_{lk} \geq r_{lk}^{th} \quad \forall l, k, \quad (31)$$

where r_{lk}^{th} is the minimum required rate for u_{lk} . The problem (31) is not convex, but can be solved by the proposed optimization framework. That is, we replace the rates by the surrogate functions in Lemma (3), which yields the following convex problem

$$\max_{\{\mathbf{x}\} \in \mathcal{X}} \sum_{lk} \lambda_{lk} \tilde{r}_{lk} \quad \text{s.t. } \tilde{r}_{lk} \geq r_{lk}^{th} \quad \forall l, k. \quad (32)$$

C. Global energy efficiency maximization

The GEE maximization problem can be written as

$$\max_{\{\mathbf{x}\} \in \mathcal{X}} \frac{\sum_{lk} r_{lk}}{LKp_c + \eta \sum_{lk} \mathbf{x}_{lk}^H \mathbf{x}_{lk}} \quad \text{s.t. } r_{lk} \geq r_{lk}^{th} \quad \forall l, k. \quad (33)$$

Replacing the rates by the lower bounds in Lemma (3), we have the following surrogate function

$$\max_{\{\mathbf{x}\} \in \mathcal{X}} \frac{\sum_{lk} \tilde{r}_{lk}}{LKp_c + \eta \sum_{lk} \mathbf{x}_{lk}^H \mathbf{x}_{lk}} \quad \text{s.t. } \tilde{r}_{lk} \geq r_{lk}^{th} \quad \forall l, k, \quad (34)$$

which is non-convex and falls into fractional-programming problems. We can obtain the global optimal solution of (34) by the Dinkelbach algorithm since the numerator of the objective function is concave in \mathbf{x}_{lk} while its denominator is convex in \mathbf{x}_{lk} [66]. The global optimal solution of (34) can be obtained by iteratively solving [66]

$$\max_{\{\mathbf{x}\} \in \mathcal{X}} \sum_{lk} \tilde{r}_{lk} - \mu^{(t,q)} \left(LKp_c + \eta \sum_{lk} \mathbf{x}_{lk}^H \mathbf{x}_{lk} \right) \quad (35a)$$

$$\text{s.t. } \tilde{r}_{lk} \geq r_{lk}^{th} \quad \forall l, k, \quad (35b)$$

and updating $\mu^{(t,q)}$ as

$$\mu^{(t,q)} = \frac{\sum_{lk} \tilde{r}_{lk} \left(\mathbf{x}_{lk}^{(t,q)} \right)}{LKp_c + \eta \sum_{lk} \mathbf{x}_{lk}^{(t,q)H} \mathbf{x}_{lk}^{(t,q)}}, \quad (36)$$

where $\mathbf{x}_{lk}^{(t,q)}$ is the initial point at the q -th iteration of the Dinkelbach algorithm, which is the solution of the previous step. We refer the readers to [66] for a detailed survey on fractional programming and the Dinkelbach algorithm.

D. Minimum-weighted energy efficiency maximization

The minimum-weighted EE maximization can be written as

$$\max_{\{\mathbf{x}\} \in \mathcal{X}, e} e \quad \text{s.t. } e_{lk} \geq e \quad \forall l, k, \quad (37a)$$

$$r_{lk} \geq r_{lk}^{th} \quad \forall l, k. \quad (37b)$$

Employing the optimization framework, we have the following surrogate optimization problem

$$\max_{\{\mathbf{x}\} \in \mathcal{X}, e} e \quad \text{s.t. } \tilde{e}_{lk} = \frac{\tilde{r}_{lk}}{p_c + \eta \mathbf{x}_{lk}^H \mathbf{x}_{lk}} \geq e \quad \forall l, k, \quad (38a)$$

$$\tilde{r}_{lk} \geq r_{lk}^{th} \quad \forall l, k, \quad (38b)$$

which is non-convex, but its global optimal solution can be obtained by the generalized Dinkelbach algorithm (GDA) since \tilde{e}_{lk} has a concave numerator and convex denominator. Applying GDA, the global optimal solution of (38) can be attained by iteratively solving

$$\max_{\{\mathbf{x}\} \in \mathcal{X}} e \quad (39a)$$

$$\text{s.t. } \tilde{r}_{lk} - \mu^{(t,q)} (p_c + \eta \mathbf{x}_{lk}^H \mathbf{x}_{lk}) \geq \alpha_{lk} e \quad \forall l, k, \quad (39b)$$

$$\tilde{r}_{lk} \geq r_{lk}^{th} \quad \forall l, k, \quad (39c)$$

and updating $\mu^{(t,q)}$ as $\mu^{(t,q)} = \min_{lk} \left\{ \tilde{e}_{lk} \left(\mathbf{x}_{lk}^{(t,q)} \right) \right\}$, where $\mathbf{x}_{lk}^{(t,q)}$ is the initial point at the q -th iteration of the Dinkelbach algorithm, which is the solution of the previous step.

IV. EXTENDING THE OPTIMIZATION FRAMEWORK TO (STAR-)RIS-ASSISTED SYSTEMS

In this section, we extend the framework in Section III to solve (24) by MM and AO for RIS-assisted systems. To this end, at the t -th iteration, we first fix the reflecting coefficients to $\{\Theta^{(t-1)}\}$ and optimize over the beamforming vectors to obtain $\{\mathbf{x}^{(t)}\}$. We then fix the beamforming vectors $\{\mathbf{x}^{(t)}\}$ and update the reflecting coefficients as $\{\Theta^{(t)}\}$. We iterate the procedure until a convergence metric is met. Note that our proposed framework converges since it produces a non-decreasing sequence in the objective function f_0 . If the feasibility set \mathcal{T} is convex, the framework falls into MM and converges to a stationary point of (24). For the initial point of the schemes, we can employ the scheme in Appendix A, similar to Section III. In the following subsections, we provide the solutions for updating $\{\mathbf{x}\}$ and $\{\Theta\}$.

A. Optimizing the beamforming vectors

In this subsection, we assume that the reflecting coefficients are fixed to $\{\Theta^{(t-1)}\}$, and we optimize over $\{\mathbf{x}\}$, which results in

$$\max_{\{\mathbf{x}\} \in \mathcal{X}} f_0 \left(\{\mathbf{x}\}, \{\Theta^{(t-1)}\} \right) \quad \text{s.t. } f_i \left(\{\mathbf{x}\}, \{\Theta^{(t-1)}\} \right) \geq 0, \forall i, \quad (40a)$$

$$r_{lk} \geq r_{lk}^{th}, \quad \forall l, k. \quad (40b)$$

This problem can be solved similar to the framework in Section III. Since it is straightforward to modify the framework in Section III to solve (40), we do not repeat the solution here.

B. Optimizing the reflecting coefficients

In this subsection, we assume that the beamforming vectors are fixed to $\{\mathbf{x}^{(t)}\}$, and we optimize only over the reflecting coefficients $\{\Theta\}$. In other words, we want to solve

$$\max_{\{\Theta\} \in \mathcal{T}} f_0 \left(\{\mathbf{x}^{(t)}\}, \{\Theta\} \right) \quad \text{s.t. } f_i \left(\{\mathbf{x}^{(t)}\}, \{\Theta\} \right) \geq 0, \forall i, \quad (41a)$$

$$r_{lk} \geq r_{lk}^{th}, \quad \forall l, k, \quad (41b)$$

where f_i s are linear functions of the rates for both spectral and energy efficiency metrics since the beamforming vectors are fixed. To solve (41), we first obtain suitable concave lower bounds for the rates. We then mention how to convexify \mathcal{T} if it is not a convex set. The rates have the same structure in the channels as in the beamforming vectors $\{\mathbf{x}\}$. Thus, we can employ a similar concave lower bound for the rates. To avoid notational confusions, we restate the lower bounds for the rates in the following corollary.

Corollary 1. A concave lower bound for r_{lk} is

$$\begin{aligned} r_{lk} \geq \hat{r}_{lk} = a_{lk} + & \frac{2\Re \left\{ \left(\mathbf{h}_{lk,l}^{(t-1)} \mathbf{x}_{lk}^{(t)} \right)^* \mathbf{h}_{lk,l} \mathbf{x}_{lk}^{(t)} \right\}}{\sigma^2 + \sum_{[ij] \neq [lk]} \left| \mathbf{h}_{lk,i}^{(t-1)} \mathbf{x}_{ij}^{(t)} \right|^2} \\ & + \frac{2Q^{-1}(\epsilon^c)}{\sqrt{n_t V_{lk}^{(t-1)}}} \frac{\sigma^2 + \sum_{[ij] \neq [lk]} \Re \left\{ \left(\mathbf{h}_{lk,i}^{(t-1)} \mathbf{x}_{ij}^{(t)} \right)^* \mathbf{h}_{lk,i} \mathbf{x}_{ij}^{(t)} \right\}}{\sigma^2 + \sum_{ij} \left| \mathbf{h}_{lk,i}^{(t-1)} \mathbf{x}_{ij}^{(t)} \right|^2} \end{aligned}$$

$$-b_{lk} \frac{\sigma^2 + \sum_{ij} \left| \mathbf{h}_{lk,i} \mathbf{x}_{ij}^{(t)} \right|^2}{\sigma^2 + \sum_{ij} \left| \mathbf{h}_{lk,i}^{(t-1)} \mathbf{x}_{ij}^{(t)} \right|^2}, \quad (42)$$

where the parameters are defined as in Lemma 3.

Note that the concave lower bound in Corollary 1 is quadratic in $\{\Theta\}$. Plugging the concave lower bound \hat{r}_{lk} into (41), we have the following surrogate optimization problem

$$\max_{\{\Theta\} \in \mathcal{T}} \hat{f}_0 \left(\left\{ \mathbf{x}^{(t)} \right\}, \{\Theta\} \right) \text{ s.t. } \hat{f}_i \left(\left\{ \mathbf{x}^{(t)} \right\}, \{\Theta\} \right) \geq 0, \forall i, \quad (43a)$$

$$\hat{r}_{lk} \geq r_{lk}^{th}, \forall l, k. \quad (43b)$$

The optimization problem (43) is convex if the feasibility set \mathcal{T} is convex, i.e., when considering \mathcal{T}_U for regular RIS and \mathcal{T}_{SU} for STAR-RIS. In this case, the proposed framework converges to a stationary point of (24). Unfortunately, the feasibility sets \mathcal{T}_I , \mathcal{T}_C , \mathcal{T}_{SI} , and \mathcal{T}_{SN} are not convex. To convexify them, we employ a suboptimal approach as described in the following. It should be emphasized that although the convergence of our proposed framework is guaranteed for all the RIS feasibility sets, we do not make any claim on the optimality of our framework for the non-convex RIS feasibility sets.

1) *Feasibility set \mathcal{T}_I* : In this case, we have the non-convex constraint $|\theta_{mn}| = 1$ for all m, n , which can be rewritten as

$$|\theta_{mn}|^2 \leq 1, \quad (44)$$

$$|\theta_{mn}|^2 \geq 1, \quad (45)$$

for all m, n . The constraint (44) is convex. However, the constraint (45) makes the problem (43) non-convex since $|\theta_{mn}|^2$ is a convex function, rather than being concave. Thus, we employ convex-concave procedure (CCP) and approximate (45) by a linear constraint as in [35, Eq. (38)]. We then also relax the constraint in [35, Eq. (39)] by introducing $\epsilon > 0$ as

$$|\theta_{mn}|^2 \geq |\theta_{mn}^{(t-1)}|^2 - 2\Re\{\theta_{mn}^{(t-1)*}(\theta_{mn} - \theta_{mn}^{(t-1)})\} \geq 1 - \epsilon, \quad (46)$$

for all m, n . Plugging (44) and (46) into (43), we have the following convex optimization problem

$$\max_{\{\Theta\}} \hat{f}_0 \left(\left\{ \mathbf{x}^{(t)} \right\}, \{\Theta\} \right) \text{ s.t. } \hat{f}_i \left(\left\{ \mathbf{x}^{(t)} \right\}, \{\Theta\} \right) \geq 0, \forall i, \quad (47a)$$

$$\hat{r}_{lk} \geq r_{lk}^{th}, \forall l, k, \quad (47b)$$

$$(46), (44) \forall m, n. \quad (47c)$$

Since (47) is convex, it can be solved efficiently by numerical tools. Let us call the solution of (47) as $\{\hat{\Theta}\}$. Although the relaxation in (46) makes the convergence of our framework faster, it may make $\{\hat{\Theta}\}$ infeasible. To obtain a feasible point, we project $\{\hat{\Theta}\}$ to \mathcal{T}_I by normalizing $\{\hat{\Theta}\}$ as $\{\hat{\Theta}^{\text{new}}\}$, i.e.,

$$\hat{\theta}_{mn}^{\text{new}} = \frac{\hat{\theta}_{mn}}{|\hat{\theta}_{mn}|}, \quad \forall m, n. \quad (48)$$

To ensure the convergence of our scheme, we update $\{\Theta\}$ as

$$\{\Theta^{(t)}\} = \begin{cases} \{\hat{\Theta}^{\text{new}}\} & \text{if } f \left(\left\{ \mathbf{P}^{(t)} \right\}, \{\hat{\Theta}^{\text{new}}\} \right) \geq \\ & f \left(\left\{ \mathbf{P}^{(t)} \right\}, \{\Theta^{(t-1)}\} \right) \\ \{\Theta^{(t-1)}\} & \text{Otherwise.} \end{cases} \quad (49)$$

This updating rule guarantees convergence by generating a sequence of non-decreasing objective functions.

2) *Feasibility set \mathcal{T}_C* : To convexify \mathcal{T}_C , we first relax the relationship between the phase and amplitude of reflecting components. In other words, we consider them as independent optimization parameters. This relaxation yields (44) and

$$|\theta_{mn}|^2 \geq |\theta|_{\min}^2, \quad (50)$$

for all m, n . Now, the problem is similar to convexifying the feasibility set \mathcal{T}_C . That is, we employ CCP to find a suitable linear lower bound for $|\theta_{mn}|^2$ as

$$|\theta_{mn}^{(t-1)}|^2 + 2\Re\left(\theta_{mn}^{(t-1)}(\theta_{mn} - \theta_{mn}^{(t-1)})^*\right) \geq |\theta|_{\min}^2, \quad (51)$$

which results in the following convex surrogate optimization problem

$$\max_{\{\Theta\}} \hat{f}_0 \left(\left\{ \mathbf{x}^{(t)} \right\}, \{\Theta\} \right) \text{ s.t. } \hat{f}_i \left(\left\{ \mathbf{x}^{(t)} \right\}, \{\Theta\} \right) \geq 0, \forall i, \quad (52a)$$

$$\hat{r}_{lk} \geq r_{lk}^{th}, \forall l, k, \quad (52b)$$

$$(51), (44) \forall m, n. \quad (52c)$$

Due to the relaxation of the dependency of the amplitude and phase of reflecting components, the solution of (52), i.e., $\{\Theta^{(*)}\}$ may be infeasible. To generate a feasible solution, we project $\{\Theta^{(*)}\}$ into \mathcal{T}_C as

$$\{\hat{\Theta}^{\text{new}}\} = \mathcal{F}(\angle\{\Theta^{(*)}\}), \quad (53)$$

where \mathcal{F} is defined as in (8), and update $\{\Theta\}$ according to (49), which guarantees the convergence.

3) *STAR-RIS with mode switching and feasibility set \mathcal{T}_{SI} or \mathcal{T}_{SN}* : In our proposed mode switching (MS) approach, we randomly divide the reflecting components into two sets: reflecting set and transmitting set. This scheme converts each STAR-RIS into two regular RISs. Thus, the MS scheme can be obtained similar to considering two RISs with the feasibility set \mathcal{T}_I , instead of each STAR-RIS.

4) *STAR-RIS with time switching and feasibility set \mathcal{T}_{SI} or \mathcal{T}_{SN}* : In our proposed time switching (TS) approach, we divide each time slot into two sub-slots. In the first sub-slot, all the RIS components operate in the reflection mode, while in the second sub-slot, they all operate in the transmission mode. In both sub-slots, each STAR-RIS operates similar to a regular RIS with feasibility set \mathcal{T}_I . Thus, we can employ the proposed algorithm for regular RIS with \mathcal{T}_I to update the RIS components in each sub-slot.

5) *Feasibility set \mathcal{T}_{SI} (STAR-RIS with energy splitting)*: In the energy splitting (ES) approach, each RIS component can simultaneously reflect and transmit, which makes it impossible to model STAR-RIS as a set of regular RISs. Thus, we have to directly tackle the constraint $|\theta_{mn}^t|^2 + |\theta_{mn}^r|^2 = 1$, which can be rewritten as

$$|\theta_{mn}^t|^2 + |\theta_{mn}^r|^2 \leq 1, \quad (54)$$

$$|\theta_{mn}^t|^2 + |\theta_{mn}^r|^2 \geq 1. \quad (55)$$

The former constraint is convex, but the latter is not since $|\theta_{mn}^t|^2$ and $|\theta_{mn}^r|^2$ are convex functions. Thus, we can employ CCP to approximate (55) by a linear constraint similar to the feasibility set \mathcal{T}_I . To make the convergence faster, we also relax (55) by introducing a positive variable ϵ as

$$|\theta_{mn}^{r(t-1)}|^2 + 2\Re\left(\theta_{mn}^{r(t-1)}(\theta_{mn}^r - \theta_{mn}^{r(t-1)})^*\right) + |\theta_{mn}^{t(t-1)}|^2 + 2\Re\left(\theta_{mn}^{t(t-1)}(\theta_{mn}^t - \theta_{mn}^{r(t-1)})^*\right) \geq 1 - \epsilon. \quad (56)$$

Substituting (54) and (56) in (43), we have the following convex surrogate optimization problem

$$\max_{\{\Theta\}} \hat{f}_0\left(\{\mathbf{x}^{(t)}\}, \{\Theta\}\right) \text{ s.t. } \hat{f}_i\left(\{\mathbf{x}^{(t)}\}, \{\Theta\}\right) \geq 0, \forall i, \quad (57a)$$

$$\hat{r}_{lk} \geq r_{lk}^{th}, \forall l, k, \quad (57b)$$

$$(54), (56) \forall m, n. \quad (57c)$$

Due to the relaxation in (56), the solution of (56), i.e., $\Theta_m^{r(*)}$ and $\Theta_m^{t(*)}$, may not be feasible. Thus, we first project $\Theta_m^{r(*)}$ and $\Theta_m^{t(*)}$ into \mathcal{T}_{SI} as

$$\hat{\theta}_{mn}^t = \frac{\theta_{mn}^{t(*)}}{\sqrt{|\theta_{mn}^{t(*)}|^2 + |\theta_{mn}^{r(*)}|^2}}, \quad \hat{\theta}_{mn}^r = \frac{\theta_{mn}^{r(*)}}{\sqrt{|\theta_{mn}^{t(*)}|^2 + |\theta_{mn}^{r(*)}|^2}}, \quad (58)$$

for all m, n . Finally, we update Θ_m^r and Θ_m^t as

$$\{\Theta^{r(t)}, \Theta^{t(t)}\} = \begin{cases} \{\hat{\Theta}^r, \hat{\Theta}^t\} & \text{if } f\left(\{\mathbf{P}^{(t)}\}, \{\hat{\Theta}^r, \hat{\Theta}^t\}\right) \geq \\ & f\left(\{\mathbf{P}^{(t)}\}, \{\Theta^{(t-1)}\}\right) \\ \{\Theta^{(t-1)}\} & \text{Otherwise,} \end{cases} \quad (59)$$

where $\{\Theta^{(t-1)}\} = \{\Theta^{r(t-1)}, \Theta^{t(t-1)}\}$. This updating policy ensures the convergence.

6) Feasibility set \mathcal{T}_{SN} (STAR-RIS with energy splitting):

The feasibility set \mathcal{T}_{SN} is a subset of \mathcal{T}_{SI} . In other words, \mathcal{T}_{SN} includes the two convex constraints in (12) and (13), in addition to the constraint $|\theta_{mn}^t|^2 + |\theta_{mn}^r|^2 = 1$. Since (12) and (13) are convex constraints, we should handle only the non-convex constraint $|\theta_{mn}^t|^2 + |\theta_{mn}^r|^2 = 1$, which can be done similar to our algorithm for the feasibility set \mathcal{T}_{SI} . That is, we have to solve the following convex surrogate problem:

$$\max_{\{\Theta\}} \hat{f}_0\left(\{\mathbf{x}^{(t)}\}, \{\Theta\}\right) \text{ s.t. } \hat{f}_i\left(\{\mathbf{x}^{(t)}\}, \{\Theta\}\right) \geq 0, \forall i, \quad (60a)$$

$$\hat{r}_{lk} \geq r_{lk}^{th}, \forall l, k, \quad (60b)$$

$$(12), (14), (54), (56) \forall m, n. \quad (60c)$$

The solution of (60) may be infeasible because of the relaxation in (56). Thus, we normalize the solution according to (58) and update Θ_m^r and Θ_m^t according to the rule in (59) to ensure the convergence.

Algorithm I Our algorithm for MWRM with STAR-RIS and \mathcal{T}_{SN} .

Initialization

Set $\epsilon, t = 1, \{\mathbf{x}\} = \{\mathbf{x}^{(0)}\}$, and $\{\Theta\} = \{\Theta^{(0)}\}$

While $\left(\min_{lk} \frac{r_{lk}^{(t)}}{\lambda_{lk}} - \min_{lk} \frac{r_{lk}^{(t-1)}}{\lambda_{lk}}\right) / \min_{lk} \frac{r_{lk}^{(t-1)}}{\lambda_{lk}} \geq \epsilon$

Optimizing over $\{\mathbf{P}\}$ by fixing $\{\Theta^{(t-1)}\}$

Obtain $\hat{r}_{lk}^{(t-1)}$ based on (27) in Lemma 3

Compute $\{\mathbf{x}^{(t)}\}$ by solving (30)

Optimizing over $\{\Theta\}$ by fixing $\{\mathbf{P}^{(t-1)}\}$

Obtain $\hat{r}_{lk}^{(t-1)}$ based on (42) in Corollary 1

Compute $\Theta_m^{r(*)}$ and $\Theta_m^{t(*)}$ by solving (60)

Update $\{\Theta^{(t)}\}$ based on the rule in (59)

$$t = t + 1$$

End (While)

Return $\{\mathbf{P}^*\}$ and $\{\Theta^*\}$.

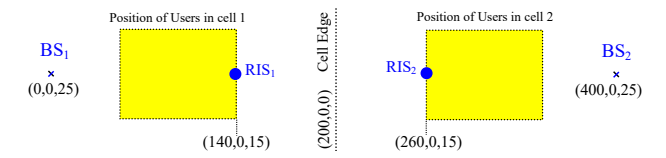


Fig. 5: System topology in simulations.

C. Discussions on different STAR-RIS modes

It can be expected that the ES approach outperforms the MS and/or TS approaches since it includes the MS and/or TS approaches as special cases. In the ES approach, each RIS component can simultaneously reflect and transmit signals, while in the MS and/or TS approaches, each RIS component either transmits or reflects at a time. In other words, the solutions of the MS and/or TS schemes are feasible, but possibly suboptimal for the ES scheme. Indeed, in the ES scheme, it may happen that a set of RIS components work only in the transmission mode while the remaining components operate in the reflection mode, which is the same as in the MS approach. Additionally, if we allow time slot sharing as it is the case in the TS approach, it may happen that in the ES approach, all RIS components operate in the transmission mode in the first time slot, while they all operate only in the reflection mode in the next time slot, which is the same as in the TS approach. As a result, an optimal ES approach never performs worse than any MS/TS scheme.

We can also compare ES, MS and TS based on the coverage of STAR-RIS. The ES and MS can simultaneously provide a 360° coverage. However, the TS approach can cover only a subspace (either reflection or transmission spaces), which may restrict the practicality of the TS mode especially in URLLC systems in which each user constantly requires an ultra-reliable communication with a very low latency. Indeed, since the STAR-RIS with the TS mode can cover only a subset of users in each sub-slot, some users may not receive any signal from the STAR-RIS at a time slot. This issue is more critical when the users are close to the cell edge, which means that they may have a very weak link, and they would be in outage without the assistance of the STAR-RIS. In such scenarios and in the presence of a very stringent latency constraint, the TS approach may not be a feasible option. However, if the latency constraint is more relaxed and/or the users are not in outage without the assistance of STAR-RIS, the TS approach can be still beneficial. Another drawback of the TS mode is that we have to solve the corresponding optimization problems twice for the coherence time of the channels, which results in inefficient TS mode in fast fading systems.

V. NUMERICAL RESULTS

In this section, we present some numerical results for the considered optimization problems. We consider a two-cell BC with K users in each cell as shown in Fig. 5, unless it is mentioned otherwise. We consider one RIS in each cell since it has been shown that a distributed implementation of RIS can outperform a collocated implementation [34]. The heights of BSs, RISs and users are, respectively, 25, 15, and 1.5 meters. The BSs are located at (0, 0, 25) and (400, 0, 25) while RISs

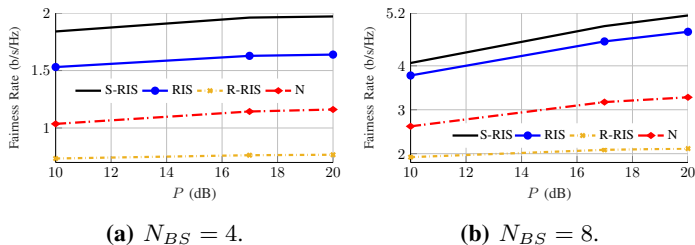


Fig. 6: The average fairness rate versus P for $NRIS = 20$, $L = 2$, $K = 4$, $M = 2$, $n_t = 256$ bits, and $\epsilon^c = 10^{-5}$.

are located close to the users at $(140, 0, 15)$ and $(260, 0, 15)$. The K users, in each cell, are located in a square with a side 20 meters exactly in front of the RIS. We represent the power budget of BSs with P . We assume that the channels through RISs are line of sight (LoS), while the direct channels are non-LoS (NLoS). It means that the links through RISs follow the Rician fading, but the direct links experience a Rayleigh fading. The propagation parameters are chosen as in [34].

As indicated, to the best of our knowledge, there is no other work that considers EE metrics and/or STAR-RIS in RIS-assisted URLLC systems with FBL. Thus, we consider the following schemes in the simulations:

- **S-RIS** refers to the Shannon rate in RIS-assisted systems with the feasibility set \mathcal{T}_I .
- **RIS** refers to the proposed scheme for RIS-assisted systems with the feasibility set \mathcal{T}_I .
- **RIS_U** (or **RIS_C**) refers to the proposed scheme for RIS-assisted systems with the feasibility set \mathcal{T}_U (or \mathcal{T}_C).
- N refers to the scheme without RIS.
- **R-RIS** refers to the proposed scheme for RIS-assisted systems with random reflecting coefficients.
- **ST-RIS_{EX}** refers to the proposed scheme for STAR-RIS-assisted systems with energy splitting and the feasibility set \mathcal{T}_{SX} , where X can be U , I and N for modeling the feasibility set \mathcal{T}_{SU} , \mathcal{T}_{SI} , and \mathcal{T}_{SN} , respectively.
- **ST-RIS_M** (or **ST-RIS_T**) refers to the proposed scheme for STAR-RIS-assisted systems with mode (or time) switching and the feasibility set \mathcal{T}_{SI} .

In the following, we consider the maximization of the minimum rate, sum rate, global EE and minimum EE of users in separate subsections. Through numerical examples, we investigate the impact of various parameters on the performance of RIS and/or STAR-RIS. These parameters are the power budget of BSs, number of BS antennas, number of users per cell, packet length, and decoding error probability. We discuss how these parameters may affect on the FBL rate as well as on the gap between the FBL rate and the Shannon rate.

A. Minimum-weighted rate maximization

In this subsection, we provide some numerical results for maximizing the minimum rate by considering the effect of different parameters. We call the minimum rate of users as the fairness rate since all users mostly achieve the same rate if we maximize the minimum rate.

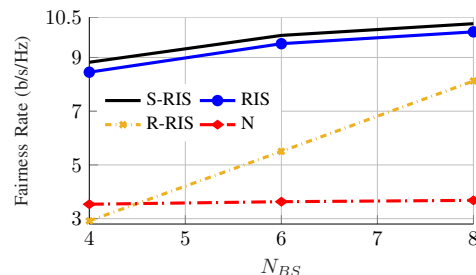


Fig. 7: The average fairness rate versus N_{BS} for $P = 20\text{dB}$, $N_{RIS} = 20$, $L = 2$, $K = 2$, $M = 2$, $n_t = 200$, and $\epsilon^c = 0.001$.

1) *Impact of power budget*: Fig. 6 shows the average fairness rate versus the power budget of BSs for $N_{RIS} = 20$, $L = 2$, $K = 4$, $M = 2$, $n_t = 256$, $\epsilon^c = 10^{-5}$, and different number of BS antennas. As can be observed, RIS can significantly increase the average fairness rate for the considered N_{BS} if the reflecting coefficients are optimized properly. Interestingly, we can observe that RIS performs worse than the systems without RIS when the reflecting coefficients are chosen randomly. This indicates the importance of optimizing RIS components. Additionally, the performance gap between the achievable rate with FBL and the Shannon rate decreases with N_{BS} when the other parameters are fixed. It happens since the SINR may be improved by increasing the number of transmit antennas. It means that the performance gap is expected to be higher when we operate in [highly] overloaded systems, i.e., when the number of users per cell is equal to or higher than the number of BS antennas.

2) *Impact of transmit antennas:* Fig. 7 shows the average fairness rate versus N_{BS} for $P = 20\text{dB}$, $N_{RIS} = 20$, $L = 2$, $K = 2$, $M = 2$, $n_t = 200$, and $\epsilon^c = 0.001$. As expected, the average fairness rate increases with the number of BS antennas. We can also observe that RIS can considerably increase the average minimum rate of users, and the benefits of RIS slightly increase with N_{BS} . Interestingly, we observe that the benefits of optimizing the reflecting coefficients decrease with N_{BS} even though they are still significant. The reason is that, the effective channel gains may be more dependent on the reflecting coefficient when N_{BS} is low. Furthermore, we observe that the gap between the Shannon rate and the FBL rate slightly decrease with N_{BS} , which is in line with the results in Fig. 6. Moreover, we observe that the performance gap between the Shannon rate and the FBL rate is much lower than when $\epsilon = 10^{-5}$ (see Fig. 6), which implies that we should expect higher performance loss comparing to the Shannon if we require ultra-reliable communication.

3) *Impact of number of users per cell:* Fig. 8 shows the average fairness rate versus K for $P = 20\text{dB}$, $N_{RIS} = 20$, $L = 2$, $N_{BS} = 8$, $M = 2$, $n_t = 200$, and $\epsilon^c = 0.001$. As can be observed, the fairness rate significantly decreases with K . RIS can improve the system performance considerably when $K \leq 4$. However, the benefits of RIS decrease with K and become almost negligible for $K = 6$ in this particular example. The reason is that, the number of RIS components per user decreases when there are more users in the system. Thus, we have to increase the number of RIS components

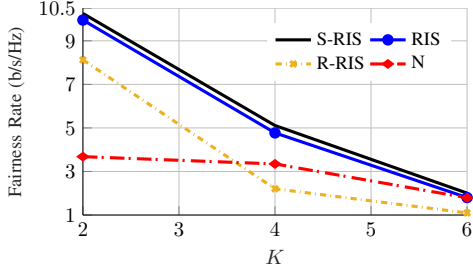


Fig. 8: The average fairness rate versus K for $P = 10\text{dB}$, $N_{RIS} = 20$, $N_{BS} = 8$, $L = 2$, $K = 2$, $M = 2$, $n_t = 200$, and $\epsilon^c = 0.001$.

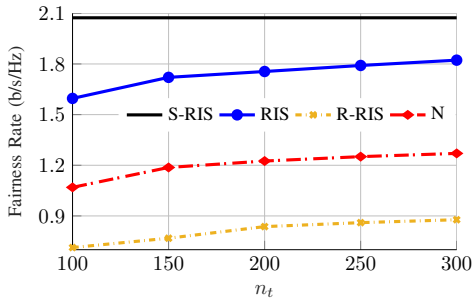


Fig. 9: The average fairness rate versus n_t for $\epsilon = 10^{-3}$, $N_{RIS} = 20$, $L = 2$, $K = 4$, $M = 2$, $P = 100$, and $N_{BS} = 4$.

to compensate for the increment of the number of users. Furthermore, we observe that optimizing over the reflecting coefficients is more important when the number of users increases. Indeed, RIS with random reflecting coefficients may even perform much worse than the systems without RIS when K grows. Finally, we also observe that the relative mismatch between the Shannon rate and the FBL rate increases with K . The mismatch is around 3% for $K = 2$, 7% for $K = 4$, and 12% for $K = 6$. As indicated before, it happens since the effective SINR decreases with K , which in turn yields the further decrements in the FBL rate. Note that the gap increase if we reduce n_t and/or ϵ^c as discussed in the following.

4) *Impact of packet lengths:* Fig. 9 shows the average fairness rate versus n_t for $N_{BS} = 4$, $N_{RIS} = 20$, $L = 2$, $K = 4$, $M = 2$, $P = 100$, and $\epsilon^c = 0.001$. As can be observed, by increasing the packet length, the gap between the Shannon rate and achievable rate by (18) decreases. Of course, n_t is not the only important parameter, and there are other effective parameters such as ϵ^c and SINR that can have a high impact on the performance and accuracy of the normal approximation in (18) as discussed before.

5) *Impact of ϵ^c :* Fig. 10 shows the average fairness rate versus ϵ^c for $n_t = 200$, $N_{RIS} = 20$, $L = 2$, $K = 4$, $M = 2$, and $N_{BS} = 4$. As can be observed, the average rate increases with ϵ^c . In other words, the lower the decoding error probability is, the lower the average rate is. Thus, if we work on ultra-reliable regime with FBL, we have to tolerate some performance loss in the data rate. The more reliable the communication is, the less data rate we can achieve. We can also observe in Fig. 10 that RIS can significantly increase the average fairness rate of the system and consequently, for a given date rate, it can highly improve the reliability of the

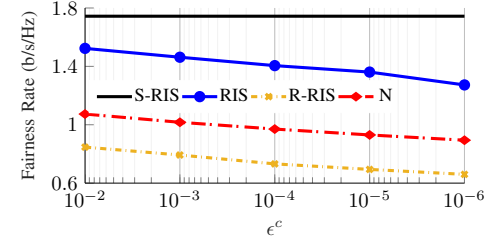


Fig. 10: The average fairness rate versus ϵ for $n_t = 200$, $N_{RIS} = 20$, $L = 2$, $K = 4$, $M = 2$, $P = 10$, and $N_{BS} = 4$.

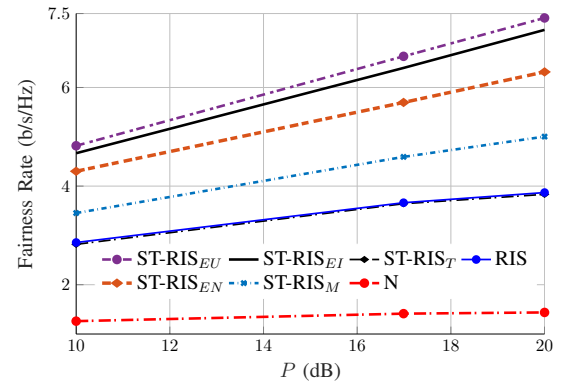


Fig. 11: The average fairness rate versus P for $N_{BS} = 6$, $N_{RIS} = 60$, $L = 1$, $K = 6$, $M = 1$, $n_t = 200$, and $\epsilon^c = 0.001$.

communication link.

6) *STAR-RIS:* Now we compare the performance of a regular RIS with a STAR-RIS. To this end, we consider a single-cell BC with K users. We assume that the regular RIS can assist only a half of users. In other words, only $K/2$ users are covered by the regular RIS, and the other $K/2$ users do not receive a signal from the regular RIS. However, the STAR-RIS can assist all users since it provides a 360° coverage. We assume that $K/2$ users are in the reflection space of the STAR-RIS, while the other $K/2$ users are in the transmission space of the STAR-RIS. We assume that both the regular and STAR-RIS have the same number of components, i.e., N_{RIS} . We consider three different strategies for the STAR-RIS. First, half of the RIS components operate only in the reflection mode, and the other half operate only in the transmission mode. We refer to this scheme as the mode switching, similar to [37]. Second, we assume that all RIS components operate simultaneously in the transmission and reflection modes, which is referred to as the energy splitting mode. Third, we divide each time slot into two sub-slots and assume that all RIS components operate in reflection mode in the first sub-slot, while they all operate in transmission mode in the next sub-slot, which is referred to as the time switching mode.

Fig. 11 shows the average fairness rate versus P for $N_{BS} = 6$, $N_{RIS} = 60$, $L = 1$, $K = 6$, $M = 1$, $n_t = 200$, and $\epsilon^c = 0.001$. As can be observed, the regular RIS can highly improve the system performance even though it assists only a half of users. The average fairness rate for systems without RIS slightly increases with power budget; however, the fairness rate of RIS-assisted systems (either STAR or regular) almost

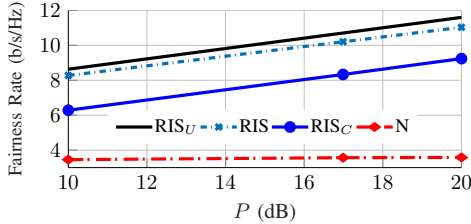


Fig. 12: The average fairness rate versus P for $N_{BS} = 8$, $N_{RIS} = 40$, $L = 2$, $K = 2$, $M = 2$, $n_t = 256$, and $\epsilon^c = 10^{-5}$.

linearly increases with the power budget. The reason is that the system is interference-limited, and the power budget increment is not necessarily equivalent to SINR improvement. Since the system is not highly overloaded, RIS can manage part of interference, which significantly improves the effective SINR. Additionally, the users are in the cell edge, which implies that they have a relatively weak direct link. Thus, RIS can considerably improve the channel gain, which in turn provide a significant gain, especially when the power budget is high.

We also observe that the STAR-RIS can outperform the regular RIS with both the MS and ES schemes. However, the STAR-RIS with TS cannot provide any benefit over regular RIS in this particular example since the TS mode covers only reflection or transmission spaces at each time sub-slot, which implies that the TS mode can assist only a half of users in each sub-slot, similar to the regular RIS. Indeed, the TS mode cannot provide a 360° coverage simultaneously, which restricts its applicability in this particular scenario. Moreover, we observe that the STAR-RIS with the ES scheme and different feasibility sets outperforms the MS scheme with the feasibility set \mathcal{T}_{SI} . The reason is that the MS scheme can be seen as a lower bound for the performance of STAR-RIS with the ES scheme since the ES scheme encompasses the MS scheme. Finally, we observe that the ES scheme with the feasibility set \mathcal{T}_{SI} performs very close to the ES scheme with the feasibility set \mathcal{T}_{SU} , which can be considered as an upper bound for the system performance.

7) *Impact of the feasibility sets:* Fig. 12 shows the average fairness rate versus P for $N_{BS} = 8$, $N_{RIS} = 40$, $L = 2$, $K = 2$, $M = 2$, $n_t = 256$, and $\epsilon^c = 10^{-5}$. As expected, the feasibility set \mathcal{T}_U outperforms the other feasibility sets. However, the feasibility set \mathcal{T}_I performs very close to the upper bound performance of a passive RIS, which is given by \mathcal{T}_U . Note that our proposed scheme for the feasibility set \mathcal{T}_U converges to a stationary point of the original problem. Thus, the gap between the upper bound with \mathcal{T}_U and our proposed scheme with \mathcal{T}_I can be seen as an upper bound for the mismatch between our proposed algorithm and a scheme, which attains a stationary point of the original problem.

B. Weighted-sum rate maximization

In the previous subsections, we consider the impact of different parameters in the system performance. It can be expected that we observe a similar behavior if we change the objective function. Thus, in this subsection, we provide only one numerical example. Fig. 13 shows the average sum rate

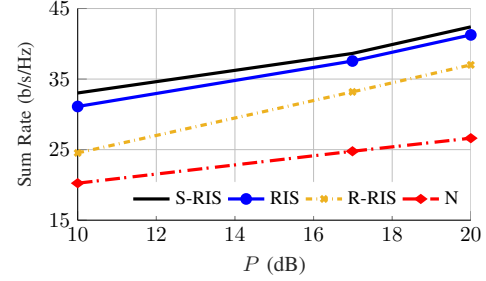


Fig. 13: The average sum rate versus P for $N_{BS} = 10$, $N_{RIS} = 20$, $L = 2$, $K = 2$, $M = 2$, $n_t = 200$, and $\epsilon^c = 0.001$.

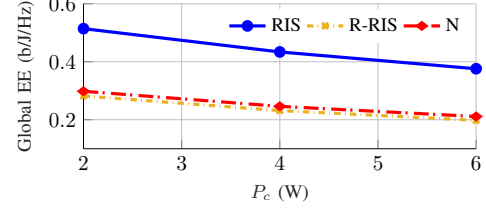


Fig. 14: The average GEE versus p_c for $N_{BS} = 4$, $N_{RIS} = 20$, $L = 2$, $K = 2$, $M = 2$, $n_t = 200$, and $\epsilon^c = 0.001$.

versus P for $N_{BS} = 10$, $N_{RIS} = 20$, $L = 2$, $K = 2$, $M = 2$, $n_t = 200$, and $\epsilon^c = 0.001$. As can be observed, RIS can significantly increase the sum rate of the system. Even an RIS with random components can highly improve the system performance. We also observe that there is a small gap between the rate with FBL and the Shannon rate, and the gap decreases with the power budget. The reason is that, the mismatch between the rate in (18) and the Shannon rate decreases with SINR, and the increment in power budget may result in SINR enhancement since the system is not overloaded. Note that the gap is expected to increase if we employ a shorter packet length or operate in a lower decoding error probability.

C. Global energy efficiency maximization

Fig. 14 shows the average GEE versus p_c for $N_{BS} = 4$, $N_{RIS} = 20$, $L = 2$, $K = 2$, $M = 2$, $n_t = 200$, and $\epsilon^c = 0.001$. In this figure, we assume that the power consumption of each RIS is 1 W. Thus, the effective p_c for users in systems without RIS is actually $p_c - 1/K$ W. Note that p_c is the constant power consumption by the devices and is different from the transmission power. We can observe through Fig. 15 that RIS can highly increase the average GEE of the system if the RIS components are properly optimized. However, if the RIS components are randomly chosen, it may happen that RIS may worsen the system performance in this particular example, which is in line with the results in Fig. 6a.

D. Minimum-weighted energy efficiency maximization

Fig. 15 shows the average fairness EE versus p_c for $N_{BS} = 4$, $N_{RIS} = 20$, $L = 2$, $K = 2$, $M = 2$, $n_t = 200$, and $\epsilon^c = 0.001$. Similar to Fig. 14, we consider the power consumption of each RIS as 1 W. As can be observed, RIS can significantly improve the EE of the system if the reflecting

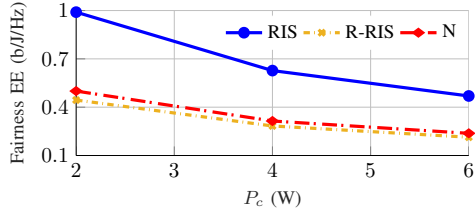


Fig. 15: The average fairness EE versus p_c for $N_{BS} = 4$, $N_{RIS} = 20$, $L = 2$, $K = 2$, $M = 2$, $n_t = 200$, and $\epsilon^c = 0.001$.

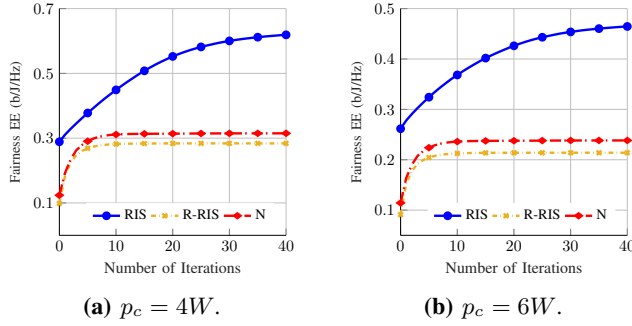


Fig. 16: The average fairness EE versus number of iterations for $N_{BS} = 4$, $N_{RIS} = 20$, $L = 2$, $K = 2$, $M = 2$, $n_t = 200$, and $\epsilon^c = 0.001$.

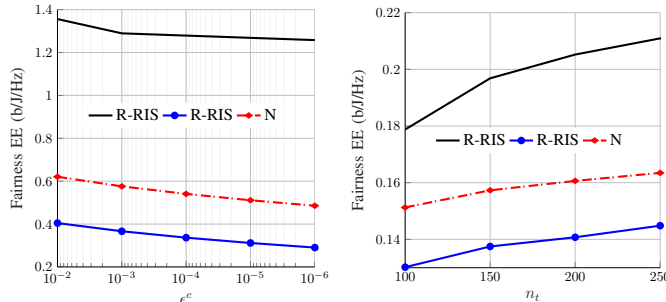


Fig. 17: The average fairness EE versus ϵ^c and n_t for $N_{BS} = 4$, $N_{RIS} = 20$, $L = 2$, $K = 2$, $M = 2$.

coefficients are properly optimized. Note that RIS with random reflecting coefficients may not provide any benefits in this particular example, which shows the importance of optimizing the reflecting coefficients. We also observe this in Fig. 6a and Fig. 14.

Fig. 16 shows the average fairness EE versus the number of iterations for $N_{BS} = 4$, $N_{RIS} = 20$, $L = 2$, $K = 2$, $M = 2$, $n_t = 200$, and $\epsilon^c = 0.001$. As can be observed, RIS with random components performs worse than the algorithm for systems without RIS. However, when RIS components are properly designed, RIS can highly improve the system performance. Additionally, the algorithm for systems without RIS converges with only a few iterations, while the algorithm for RIS-assisted systems require more iterations to converge. Note that the initial point of the algorithms is given by the solution of the maximization of the minimum rate to ensure that the initial point is feasible.

Fig. 17 shows the average fairness EE versus ϵ^c and n_t for $N_{BS} = 4$, $N_{RIS} = 20$, $L = 2$, $K = 2$, $M = 2$. As can be observed, RIS can provide a significant gain for a wide range of variables if the RIS components are properly optimized. As we also observe in Section V-A with the average fairness rate as the performance metric, the system performance is improved by increasing n_t and ϵ^c . Indeed, the EE decreases if we employ a shorter packet length or if we want to operate with a more reliable link.

E. Summary

We show that RIS can significantly improve the spectral and EE of a multi-cell RIS-assisted BC with FBL and different parameters. Moreover, we show that the FBL rate is very close to the Shannon rate for underloaded systems when packet lengths are higher than 200 bits and ϵ is higher than 10^{-3} . This is also in line with the results in [13, Sec. IV.C]. Note that in underloaded systems, the number of BS antennas is higher than the number of users. Thus, the effective SINR of users is expected to be higher in underloaded systems, comparing to over-loaded systems, which decreases the gap between the FBL rate and the Shannon rate [13]. In particular, our main findings can be summarized as follows:

- For a fixed N_{RIS} , the benefits of RIS is decreasing in K since the number of RIS components per user decreases with K . To compensate for that, we have to increase the number RIS components.
- The gap between the Shannon rate and the rate by FBL decreases with SINR. It means that the gap increases with K and decreases with N_{BS} and P .
- RIS can significantly increase the data rate and EE of the system. Equivalently, for a target data rate, RIS can highly improve the reliability of the system by decreasing the error probability.

VI. CONCLUSION AND FUTURE WORK

In this paper, we proposed a general optimization framework to solve a variety of optimization problems in URLLC RIS-assisted networks with FBL. This framework can solve any optimization problem in which the objective and/or constraints are linear functions of the rates/EE of users. Additionally, the framework can be applied to any interference-limited system with TIN. We considered a multi-cell STAR-RIS-assisted BC, as an illustrative example, and specialized the framework to solve the minimum-weighted-rate, weighted-sum-rate, global-EE, and minimum-weighted-EE maximization problems. We made realistic assumptions regarding RIS (either regular or STAR-RIS). We showed that RIS can considerably improve the spectral and EE of a multi-cell MISO RIS-assisted BC with FBL if RIS components are properly optimized. Furthermore, we showed that we may operate close to the Shannon rate with a relatively short packet if the decoding error probability is not very low. Finally, we showed that a STAR-RIS can outperform a regular RIS if the regular RIS cannot cover all the users.

As future works, it can be interesting to investigate the performance of RIS in the presence of imperfect and/or only statistical CSI by extending the techniques in, e.g., [74], [75]

to a FBL regime. Moreover, the global optimal solution of the considered problems is not known, which can be another challenging line for future studies. It is also interesting to compare the performance of our techniques with machine-learning-based and/or other data-driven techniques.

VII. ACKNOWLEDGMENT

The authors would like to thank Dr. Tobias Koch for his valuable comments and discussions during the preparation of this work.

APPENDIX A INITIAL POINTS FOR THE OPTIMIZATION FRAMEWORK

In this appendix, we propose a scheme to heuristically obtain suitable initial points for the proposed optimization framework. As indicated in Section II-C, the rate $r_{l,k}$ is negative for $0 \leq \gamma_{l,k} \leq \gamma^{(0)}$, which means that $\gamma_{l,k} \leq \gamma^{(0)}$ is not a feasible point. Additionally, $r_{l,k}$ is strictly increasing in $\gamma_{l,k}$ for all feasible practical points, i.e., $\gamma_{l,k} \geq \gamma^{(0)}$. To avoid infeasible initial point and get a better performance, we set the solution of the maximization of the minimum SINR as an initial point for our framework. The maximization of the minimum SINR can be formulated as

$$\max_{\{\mathbf{x}\} \in \mathcal{X}, \{\Theta\} \in \mathcal{T}, \gamma} \gamma \quad \text{s.t. } \gamma_{lk} \geq \gamma \quad \forall l, k. \quad (61)$$

Note that for the systems without RIS, we need to optimize only over $\{\mathbf{x}\}$. However, in this appendix, we consider the most general case. The optimization problem (61) is not convex, but we can obtain a suboptimal solution of (61) by MM, AO and the generalized Dinkelbach algorithm (GDA) since it falls into fractional programming and each fraction has a quadratic numerator and denominator [66], [76]. That is, we first optimize over the beamforming vectors $\{\mathbf{x}\}$ and obtain $\{\mathbf{x}^{(t)}\}$ while the reflecting coefficients $\{\Theta\}$ are fixed to $\{\Theta^{(t-1)}\}$. Then we alternate and optimize over $\{\Theta\}$ while $\{\mathbf{x}\}$ is fixed to $\{\mathbf{x}^{(t)}\}$. Due to a space restriction, we do not provide the optimization over $\{\mathbf{x}\}$ since the problem has a structure similar to optimizing over $\{\Theta\}$. For a given $\{\mathbf{x}^{(t)}\}$, the problem (61) can be written as

$$\max_{\{\Theta\} \in \mathcal{T}, \gamma} \gamma \quad \text{s.t. } \frac{|\mathbf{h}_{lk,l} \mathbf{x}_{lk}|^2}{\sigma^2 + \sum_{\forall [ij] \neq [lk]} |\mathbf{h}_{lk,i} \mathbf{x}_{ij}|^2} \geq \gamma \quad \forall l, k, \quad (62)$$

which is a multiple-ratio FP problem in which both the numerator and denominator are quadratic functions of the channels. To solve (62), we first employ CCP to approximate the numerator of γ_{lk} for all l, k with a linear lower bound since it is a convex function. That is

$$|\mathbf{h}_{lk,l} \mathbf{x}_{lk}|^2 \geq \hat{s}_{lk}(\mathbf{h}_{lk,i}) \triangleq |\mathbf{h}_{lk,l}^{(t-1)} \mathbf{x}_{lk}^{(t)}|^2 + 2\Re \left\{ \mathbf{h}_{lk,l}^{(t-1)} \mathbf{x}_{lk}^{(t)} \left(\mathbf{h}_{lk,i} \mathbf{x}_{lk}^{(t)} - \mathbf{h}_{lk,l}^{(t-1)} \mathbf{x}_{lk}^{(t)} \right) \right\}. \quad (63)$$

Substituting (63) in (62), we have the following surrogate optimization problem

$$\max_{\{\Theta\} \in \mathcal{T}, \gamma} \gamma \quad \text{s.t. } \frac{\hat{s}_{lk}(\mathbf{h}_{lk,i})}{\sigma^2 + \sum_{\forall [ij] \neq [lk]} |\mathbf{h}_{lk,i} \mathbf{x}_{ij}|^2} \geq \gamma \quad \forall l, k, \quad (64)$$

which is non-convex, but can be solved by GDA. That is, we iteratively solve

$$\max_{\{\Theta\} \in \mathcal{T}, \gamma} \gamma \quad \text{s.t. } \hat{s}_{lk}(\cdot) - \mu^{(t,m)} \left(\sigma^2 + \sum_{\forall [ij] \neq [lk]} |\mathbf{h}_{lk,i} \mathbf{x}_{ij}|^2 \right) \geq \gamma \quad \forall l, k, \quad (65)$$

and update $\mu^{(t,m)}$ as

$$\mu^{(t,m)} = \min_{l,k} \left(\frac{\hat{s}_{lk}(\mathbf{h}_{lk,i}^{(t,m)})}{\sigma^2 + \sum_{\forall [ij] \neq [lk]} |\mathbf{h}_{lk,i}^{(t,m)} \mathbf{x}_{ij}|^2} \right),$$

where $\mathbf{h}_{lk,i}^{(t,m)}$ is the initial point at the m -th iteration of (65), which is the solution of the previous step. The optimization problem (65) is convex when \mathcal{T} is a convex set, i.e., when we consider \mathcal{T}_U for regular RIS and \mathcal{T}_{SU} for STAR-RIS. We can convexify \mathcal{T}_I , \mathcal{T}_C , \mathcal{T}_{SI} , and \mathcal{T}_{SN} similar to Section IV-B. Since it is straightforward to do so, we do not repeat them here.

APPENDIX B USEFUL INEQUALITIES

In this appendix, we provide some inequalities, which are widely used in this work. Consider real and positive variables x , \bar{x} , y and \bar{y} . Then, the following inequality holds for all x, y, \bar{x}, \bar{y} [23, Eq. (75)]

$$\sqrt{xy} \leq \frac{\sqrt{\bar{x}}}{2\sqrt{\bar{y}}} y + \frac{\sqrt{\bar{y}}}{2\sqrt{\bar{x}}} x, \quad (66)$$

For the case that $y = \bar{y} = 1$, we have

$$\sqrt{x} \leq \frac{\sqrt{\bar{x}}}{2} + \frac{x}{2\sqrt{\bar{x}}}. \quad (67)$$

Additionally, the following inequality holds for all feasible x, y, \bar{x}, \bar{y} [23, Eq. (76)]

$$\frac{x^2}{y} \geq \frac{\bar{x}}{\bar{y}} \left(2x - \frac{\bar{x}}{\bar{y}} y \right). \quad (68)$$

When x and \bar{x} are complex, (68) is modified to

$$\frac{|x|^2}{y} \geq \frac{2\Re\{\bar{x}^* x\}}{\bar{y}} - \frac{|\bar{x}|^2}{\bar{y}^2} y. \quad (69)$$

Now, consider positive real-valued variables y and \bar{y} , and complex-valued variables x and \bar{x} . Then, the following inequality holds for all feasible y, \bar{y}, x, \bar{x} [34, Lemma 2]

$$\begin{aligned} \ln \left(1 + \frac{|x|^2}{y} \right) &\geq \ln \left(1 + \frac{|\bar{x}|^2}{\bar{y}} \right) - \frac{|\bar{x}|^2}{\bar{y}} \\ &\quad + \frac{2\Re\{\bar{x}^* x\}}{\bar{y}} - \frac{|\bar{x}|^2}{\bar{y}} \frac{|x|^2 + y}{|\bar{x}|^2 + \bar{y}}. \end{aligned} \quad (70)$$

APPENDIX C PROOF OF LEMMA 3

The rate of users consists of two parts: the Shannon rate and the term related to the channel dispersion. We first obtain a concave lower-bound for the Shannon rate. To this end, we employ the inequality in (70), which gives us

$$\begin{aligned} r_{s,lk} \geq \hat{r}_{s,lk}^{(t-1)} &= \log_2 \left(1 + \gamma_{lk}^{(t-1)} \right) - \gamma_{lk}^{(t-1)} \\ &+ \frac{2\Re \left\{ \left(\mathbf{h}_{lk,l} \mathbf{x}_{lk}^{(t-1)} \right)^* \mathbf{h}_{lk,l} \mathbf{x}_{lk} \right\}}{\sigma^2 + \sum_{ij} |\mathbf{h}_{lk,i} \mathbf{x}_{ij}^{(t-1)}|^2 - |\mathbf{h}_{lk,l} \mathbf{x}_{lk}^{(t-1)}|^2} \\ &- \gamma_{lk}^{(t-1)} \frac{\sigma^2 + \sum_{ij} |\mathbf{h}_{lk,i} \mathbf{x}_{ij}^{(t-1)}|^2}{\sigma^2 + \sum_{ij} |\mathbf{h}_{lk,i} \mathbf{x}_{ij}^{(t-1)}|^2}. \end{aligned} \quad (71)$$

Now, we obtain a concave lower-bound for $-\delta_{lk}$, which is equivalent to finding a convex upper bound for $\sqrt{V_{lk}}$. Applying the inequality (67), we have

$$\sqrt{V_{lk}} \leq \frac{\sqrt{V_{lk}^{(t)}}}{2} + \frac{\gamma_{lk}}{\sqrt{V_{lk}^{(t)}} (1 + \gamma_{lk})}.$$

Replacing γ_{lk} by (19), we have

$$\begin{aligned} \delta_{lk} &= \frac{Q^{-1}(\epsilon^c)}{\sqrt{n_t}} \sqrt{V_{lk}} \leq \tilde{\delta}_{lk} = \frac{Q^{-1}(\epsilon^c) \sqrt{V_{lk}^{(t)}}}{2\sqrt{n_t}} \\ &+ \frac{Q^{-1}(\epsilon^c)}{\sqrt{n_t V_{lk}^{(t)}}} \left(1 - \underbrace{\frac{\sigma^2 + \sum_{ij \neq [lk]} |\mathbf{h}_{lk,i} \mathbf{x}_{ij}|^2}{\sigma^2 + \sum_{ij} |\mathbf{h}_{lk,i} \mathbf{x}_{ij}|^2}}_{\zeta_{lk}} \right). \end{aligned} \quad (72)$$

Unfortunately, $\tilde{\delta}_{lk}$ is not a convex function since ζ_{lk} is not concave. However, we can apply (69) to obtain a concave lower bound for ζ_{lk} (or equivalently a convex upper bound for $\tilde{\delta}_{lk}$) as

$$\begin{aligned} \zeta_{lk} &\geq 2 \frac{\sigma^2 + \sum_{ij \neq [lk]} \Re \left\{ \left(\mathbf{h}_{lk,i} \mathbf{x}_{ij}^{(t-1)} \right)^* \mathbf{h}_{lk,i} \mathbf{x}_{ij} \right\}}{\sigma^2 + \sum_{ij} |\mathbf{h}_{lk,i} \mathbf{x}_{ij}^{(t-1)}|^2} \\ &- \zeta_{lk}^{(t-1)} \frac{\sigma^2 + \sum_{ij} |\mathbf{h}_{lk,i} \mathbf{x}_{ij}^{(t-1)}|^2}{\sigma^2 + \sum_{ij} |\mathbf{h}_{lk,i} \mathbf{x}_{ij}^{(t-1)}|^2}. \end{aligned} \quad (73)$$

Substituting (73) into (72), we have

$$\begin{aligned} \delta_{lk} \leq \tilde{\delta}_{lk} \leq \hat{\delta}_{lk} &= \frac{Q^{-1}(\epsilon^c) \sqrt{V_{lk}^{(t)}}}{2\sqrt{n_t}} + \frac{Q^{-1}(\epsilon^c)}{\sqrt{n_t V_{lk}^{(t)}}} \\ &- \frac{2Q^{-1}(\epsilon^c)}{\sqrt{n_t V_{lk}^{(t)}}} \frac{\sigma^2 + \sum_{ij \neq [lk]} \Re \left\{ \left(\mathbf{h}_{lk,i} \mathbf{x}_{ij}^{(t-1)} \right)^* \mathbf{h}_{lk,i} \mathbf{x}_{ij} \right\}}{\sigma^2 + \sum_{ij} |\mathbf{h}_{lk,i} \mathbf{x}_{ij}^{(t-1)}|^2} \\ &+ \frac{Q^{-1}(\epsilon^c) \zeta_{lk}^{(t-1)}}{\sqrt{n_t V_{lk}^{(t)}}} \frac{\sigma^2 + \sum_{ij} |\mathbf{h}_{lk,i} \mathbf{x}_{ij}^{(t-1)}|^2}{\sigma^2 + \sum_{ij} |\mathbf{h}_{lk,i} \mathbf{x}_{ij}^{(t-1)}|^2}. \end{aligned} \quad (74)$$

Finally, the concave lower bound for r_{lk} is

$$r_{lk} \geq \hat{r}_{lk}^{(t-1)} = \hat{r}_{s,lk}^{(t-1)} - \hat{\delta}_{lk}^{(t-1)}. \quad (75)$$

If we substitute the values for $\hat{r}_{s,lk}^{(t-1)}$ and $\hat{\delta}_{lk}^{(t-1)}$, and simplify the equations, we can easily obtain (27).

REFERENCES

- [1] M. Vaezi, A. Azari, S. R. Khosravirad, M. Shirvanimoghaddam, M. M. Azari, D. Chasaki, and P. Popovski, "Cellular, wide-area, and non-terrestrial IoT: A survey on 5G advances and the road towards 6G," *IEEE Commun. Surv. Tutor.*, 2022.
- [2] M. Chafai, L. Bariah, S. Muhaidat, and M. Debbah, "Ten scientific challenges for 6G: Rethinking the foundations of communications theory," *arXiv preprint arXiv:2207.01843*, 2022.
- [3] M. Almekhlafi, M. A. Arfaoui, C. Assi, and A. Ghayeb, "Enabling URLLC applications through reconfigurable intelligent surfaces: Challenges and potential," *IEEE Internet Things Mag.*, vol. 5, no. 1, pp. 130–135, 2022.
- [4] G. Durisi, T. Koch, and P. Popovski, "Toward massive, ultrareliable, and low-latency wireless communication with short packets," *Proc. of the IEEE*, vol. 104, no. 9, pp. 1711–1726, 2016.
- [5] P. Popovski, Č. Stefanović, J. J. Nielsen, E. De Carvalho, M. Angelichinoski, K. F. Trillingsgaard, and A.-S. Bana, "Wireless access in ultra-reliable low-latency communication (URLLC)," *IEEE Trans. Commun.*, vol. 67, no. 8, pp. 5783–5801, 2019.
- [6] C. Bockelmann, N. Pratas, H. Nikopour, K. Au, T. Svensson, C. Stefanovic, P. Popovski, and A. Dekorsy, "Massive machine-type communications in 5G: Physical and MAC-layer solutions," *IEEE Commun. Mag.*, vol. 54, no. 9, pp. 59–65, 2016.
- [7] Q. Wu *et al.*, "Intelligent reflecting surface aided wireless communications: A tutorial," *IEEE Trans. Commun.*, vol. 69, no. 5, pp. 3313–3351, 2021.
- [8] C. Huang, *et al.*, "Holographic MIMO surfaces for 6G wireless networks: Opportunities, challenges, and trends," *IEEE Wireless Commun.*, vol. 27, no. 5, pp. 118–125, 2020.
- [9] M. Di Renzo *et al.*, "Smart radio environments empowered by reconfigurable intelligent surfaces: How it works, state of research, and the road ahead," *IEEE J. Sel. Areas Commun.*, vol. 38, no. 11, pp. 2450–2525, 2020.
- [10] M. Simsek, A. Aijaz, M. Dohler, J. Sachs, and G. Fettweis, "5G-enabled tactile internet," *IEEE J. Sel. Areas Commun.*, vol. 34, no. 3, pp. 460–473, 2016.
- [11] G. Aceto, V. Persico, and A. Pescapé, "A survey on information and communication technologies for industry 4.0: State-of-the-art, taxonomies, perspectives, and challenges," *IEEE Commun. Surv. Tutor.*, vol. 21, no. 4, pp. 3467–3501, 2019.
- [12] M. Noor-A-Rahim, F. Firayaguna, J. John, M. O. Khyam, D. P. E. Armstrong, H. Claussen, and H. V. Poor, "Towards industry 5.0: Intelligent reflecting surface (IRS) in smart manufacturing," *IEEE Commun. Mag.*, pp. 1–7, 2022.
- [13] Y. Polyanskiy, H. V. Poor, and S. Verdú, "Channel coding rate in the finite blocklength regime," *IEEE Trans. Inf. Theory*, vol. 56, no. 5, pp. 2307–2359, 2010.
- [14] T. Erseghe, "Coding in the finite-blocklength regime: Bounds based on laplace integrals and their asymptotic approximations," *IEEE Trans. Inf. Theory*, vol. 62, no. 12, pp. 6854–6883, 2016.
- [15] ———, "On the evaluation of the Polyanskiy-Poor-Verdú converse bound for finite block-length coding in AWGN," *IEEE Trans. Inf. Theory*, vol. 61, no. 12, pp. 6578–6590, 2015.
- [16] M. C. Coşkun, G. Durisi, T. Jervikits, G. Liva, W. Ryan, B. Stein, and F. Steiner, "Efficient error-correcting codes in the short blocklength regime," *Physical Communication*, vol. 34, pp. 66–79, 2019.
- [17] A. Lancho, T. Koch, and G. Durisi, "On single-antenna rayleigh block-fading channels at finite blocklength," *IEEE Trans. Inf. Theory*, vol. 66, no. 1, pp. 496–519, 2019.
- [18] P. Popovski, K. F. Trillingsgaard, O. Simeone, and G. Durisi, "5G wireless network slicing for eMBB, URLLC, and mMTC: A communication-theoretic view," *IEEE Access*, vol. 6, pp. 55 765–55 779, 2018.
- [19] S. Schiessl, M. Skoglund, and J. Gross, "NOMA in the uplink: Delay analysis with imperfect CSI and finite-length coding," *IEEE Trans. Wireless Commun.*, vol. 19, no. 6, pp. 3879–3893, 2020.
- [20] S. Schiessl, J. Gross, M. Skoglund, and G. Caire, "Delay performance of the multiuser MISO downlink under imperfect CSI and finite-length coding," *IEEE J. Sel. Areas Commun.*, vol. 37, no. 4, pp. 765–779, 2019.
- [21] S. Schiessl, H. Al-Zubaidy, M. Skoglund, and J. Gross, "Delay performance of wireless communications with imperfect CSI and finite-length coding," *IEEE Trans. Commun.*, vol. 66, no. 12, pp. 6527–6541, 2018.

[22] W. R. Ghanem, V. Jamali, Y. Sun, and R. Schober, "Resource allocation for multi-user downlink MISO OFDMA-URLLC systems," *IEEE Trans. Commun.*, vol. 68, no. 11, pp. 7184–7200, 2020.

[23] A. A. Nasir, H. D. Tuan, H. H. Nguyen, M. Debbah, and H. V. Poor, "Resource allocation and beamforming design in the short blocklength regime for URLLC," *IEEE Trans. on Wireless Commun.*, vol. 20, no. 2, pp. 1321–1335, 2020.

[24] A. Nasir, H. Tuan, H. Ngo, T. Duong, and H. Poor, "Cell-free massive MIMO in the short blocklength regime for URLLC," *IEEE Trans. Wireless Commun.*, vol. 20, no. 9, pp. 5861–5871, 2021.

[25] M. A. ElMossallamy *et al.*, "Reconfigurable intelligent surfaces for wireless communications: Principles, challenges, and opportunities," *IEEE Trans. Cogn. Commun. Netw.*, vol. 6, no. 3, pp. 990–1002, 2020.

[26] Q. Wu and R. Zhang, "Intelligent reflecting surface enhanced wireless network via joint active and passive beamforming," *IEEE Trans. Wireless Commun.*, vol. 18, no. 11, pp. 5394–5409, 2019.

[27] Y. Yang, B. Zheng, S. Zhang, and R. Zhang, "Intelligent reflecting surface meets OFDM: Protocol design and rate maximization," *IEEE Trans. on Commun.*, vol. 68, no. 7, pp. 4522–4535, 2020.

[28] C. Huang, A. Zappone, G. C. Alexandropoulos, M. Debbah, and C. Yuen, "Reconfigurable intelligent surfaces for energy efficiency in wireless communication," *IEEE Trans. Wireless Commun.*, vol. 18, no. 8, pp. 4157–4170, 2019.

[29] Q.-U.-A. Nadeem, *et al.*, "Asymptotic max-min SINR analysis of reconfigurable intelligent surface assisted MISO systems," *IEEE Trans. Wireless Commun.*, vol. 19, no. 12, pp. 7748–7764, 2020.

[30] H. Yu *et al.*, "Joint design of reconfigurable intelligent surfaces and transmit beamforming under proper and improper Gaussian signaling," *IEEE J. Sel. Areas Commun.*, vol. 38, no. 11, pp. 2589–2603, 2020.

[31] C. Pan, H. Ren, K. Wang, W. Xu, M. Elkashlan, A. Nallanathan, and L. Hanzo, "Multicell MIMO communications relying on intelligent reflecting surfaces," *IEEE Trans. Wireless Commun.*, vol. 19, no. 8, pp. 5218–5233, 2020.

[32] L. Zhang, Y. Wang, W. Tao, Z. Jia, T. Song, and C. Pan, "Intelligent reflecting surface aided MIMO cognitive radio systems," *IEEE Trans. Veh. Technol.*, vol. 69, no. 10, pp. 11445–11457, 2020.

[33] W. Ni, X. Liu, Y. Liu, H. Tian, and Y. Chen, "Resource allocation for multi-cell IRS-aided NOMA networks," *IEEE Trans. Wireless Commun.*, vol. 20, no. 7, pp. 4253–4268, 2021.

[34] M. Soleymani, I. Santamaria, and P. J. Schreier, "Improper signaling for multicell MIMO RIS-assisted broadcast channels with I/Q imbalance," *IEEE Trans. Green Commun. Netw.*, vol. 6, no. 2, pp. 723–738, 2022.

[35] M. Soleymani, I. Santamaria, E. Jorswieck, and S. Rezvani, "NOMA-based improper signaling for multicell MISO RIS-assisted broadcast channels," *arXiv preprint arXiv:2206.03795*, 2022.

[36] M. Soleymani, I. Santamaria, and E. Jorswieck, "Rate splitting in MIMO RIS-assisted systems with hardware impairments and improper signaling," *IEEE Trans. Veh. Technol.*, 2022.

[37] X. Mu, Y. Liu, L. Guo, J. Lin, and R. Schober, "Simultaneously transmitting and reflecting (STAR) RIS aided wireless communications," *IEEE Trans. Wireless Commun.*, vol. 21, no. 5, pp. 3083–3098, 2022.

[38] C. Wu, Y. Liu, X. Mu, X. Gu, and O. A. Dobre, "Coverage characterization of STAR-RIS networks: NOMA and OMA," *IEEE Commun. Lett.*, vol. 25, no. 9, pp. 3036–3040, 2021.

[39] Y. Liu, X. Mu, J. Xu, R. Schober, Y. Hao, H. V. Poor, and L. Hanzo, "STAR: Simultaneous transmission and reflection for 360 coverage by intelligent surfaces," *IEEE Wireless Commun.*, vol. 28, no. 6, pp. 102–109, 2021.

[40] J. Xu, Y. Liu, X. Mu, and O. A. Dobre, "STAR-RISs: Simultaneous transmitting and reflecting reconfigurable intelligent surfaces," *IEEE Commun. Lett.*, vol. 25, no. 9, pp. 3134–3138, 2021.

[41] J. Xu, Y. Liu, X. Mu, R. Schober, and H. V. Poor, "STAR-RISs: A correlated T&R phase-shift model and practical phase-shift configuration strategies," *IEEE J. Sel. Topics Signal Process.*, pp. 1–1, 2022.

[42] W. Ni, Y. Liu, Y. C. Eldar, Z. Yang, and H. Tian, "STAR-RIS integrated non-orthogonal multiple access and over-the-air federated learning: Framework, analysis, and optimization," *IEEE Internet Things J.*, 2022.

[43] Z. Xie, W. Yi, X. Wu, Y. Liu, and A. Nallanathan, "STAR-RIS aided NOMA in multi-cell networks: A general analytical framework with gamma distributed channel modeling," *IEEE Transactions on Communications*, 2022.

[44] Z. Zhang, J. Chen, Y. Liu, Q. Wu, B. He, and L. Yang, "On the secrecy design of STAR-RIS assisted uplink NOMA networks," *IEEE Trans. Wireless Commun.*, 2022.

[45] N. Docomo, "DOCOMO conducts world's first successful trial of transparent dynamic metasurface," 2020.

[46] Y. Li, C. Yin, T. Do-Duy, A. Masaracchia, and T. Q. Duong, "Aerial reconfigurable intelligent surface-enabled URLLC UAV systems," *IEEE Access*, vol. 9, pp. 140248–140257, 2021.

[47] T.-H. Vu, T.-V. Nguyen, D. B. da Costa, and S. Kim, "Intelligent reflecting surface-aided short-packet non-orthogonal multiple access systems," *IEEE Trans. Veh. Technol.*, vol. 71, no. 4, pp. 4500–4505, 2022.

[48] H. Ren, K. Wang, and C. Pan, "Intelligent reflecting surface-aided URLLC in a factory automation scenario," *IEEE Trans. Commun.*, vol. 70, no. 1, pp. 707–723, 2021.

[49] H. Xie, J. Xu, Y.-F. Liu, L. Liu, and D. W. K. Ng, "User grouping and reflective beamforming for IRS-aided URLLC," *IEEE Wireless Commun. Lett.*, vol. 10, no. 11, pp. 2533–2537, 2021.

[50] B. Zhang, K. Wang, K. Yang, and G. Zhang, "IRS-assisted short packet wireless energy transfer and communications," *IEEE Wireless Commun. Lett.*, vol. 11, no. 2, pp. 303–307, 2022.

[51] M. Almekhlafi, M. A. Arfaoui, M. Elhattab, C. Assi, and A. Ghayeb, "Joint resource allocation and phase shift optimization for RIS-aided eMBB/URLLC traffic multiplexing," *IEEE Trans. Commun.*, vol. 70, no. 2, pp. 1304–1319, 2022.

[52] A. Ranjha and G. Kaddoum, "URLLC facilitated by mobile UAV relay and RIS: A joint design of passive beamforming, blocklength, and uav positioning," *IEEE Internet of Things Journal*, vol. 8, no. 6, pp. 4618–4627, 2020.

[53] —, "URLLC-enabled by laser powered UAV relay: A quasi-optimal design of resource allocation, trajectory planning and energy harvesting," *IEEE Trans. Vehicular Technology*, vol. 71, no. 1, pp. 753–765, 2022.

[54] S. Dhok, P. Raut, P. K. Sharma, K. Singh, and C.-P. Li, "Non-linear energy harvesting in RIS-assisted URLLC networks for industry automation," *IEEE Trans. Commun.*, vol. 69, no. 11, pp. 7761–7774, 2021.

[55] W. R. Ghanem, V. Jamali, and R. Schober, "Joint beamforming and phase shift optimization for multicell IRS-aided OFDMA-URLLC systems," in *IEEE Wireless Commun. and Netw. Conf. (WCNC)*, 2021, pp. 1–7.

[56] M. Abughalwa, H. Tuan, D. Nguyen, H. Poor, and L. Hanzo, "Finite-blocklength RIS-aided transmit beamforming," *IEEE Trans. Veh. Technol.*, 2022.

[57] J. Scarlett, V. Y. Tan, and G. Durisi, "The dispersion of nearest-neighbor decoding for additive non-Gaussian channels," *IEEE Trans. Inf. Theory*, vol. 63, no. 1, pp. 81–92, 2016.

[58] Y. Sun, P. Babu, and D. P. Palomar, "Majorization-minimization algorithms in signal processing, communications, and machine learning," *IEEE Trans. Signal Process.*, vol. 65, no. 3, pp. 794–816, 2017.

[59] J. Zuo, Y. Liu, Z. Qin, and N. Al-Dhahir, "Resource allocation in intelligent reflecting surface assisted NOMA systems," *IEEE Trans. Commun.*, vol. 68, no. 11, pp. 7170–7183, 2020.

[60] X. Mu, Y. Liu, L. Guo, J. Lin, and N. Al-Dhahir, "Exploiting intelligent reflecting surfaces in NOMA networks: Joint beamforming optimization," *IEEE Trans. Wireless Commun.*, vol. 19, no. 10, pp. 6884–6898, 2020.

[61] G. Yang, X. Xu, Y.-C. Liang, and M. Di Renzo, "Reconfigurable intelligent surface-assisted non-orthogonal multiple access," *IEEE Trans. Wireless Commun.*, vol. 20, no. 5, pp. 3137–3151, 2021.

[62] T. Jiang and W. Yu, "Interference nulling using reconfigurable intelligent surface," *IEEE J. Sel. Areas Commun.*, 2022.

[63] Y. Liu, X. Mu, R. Schober, and H. V. Poor, "Simultaneously transmitting and reflecting (STAR)-RISs: A coupled phase-shift model," in *Proc. IEEE Int. Conf. Commun. (ICC)*. IEEE, 2022, pp. 2840–2845.

[64] S. Abeywickrama, R. Zhang, Q. Wu, and C. Yuen, "Intelligent reflecting surface: Practical phase shift model and beamforming optimization," *IEEE Trans. Commun.*, vol. 68, no. 9, pp. 5849–5863, 2020.

[65] A. Lancho, J. Östman, G. Durisi, T. Koch, and G. Vazquez-Vilar, "Saddlepoint approximations for short-packet wireless communications," *IEEE Trans. Wireless Commun.*, vol. 19, no. 7, pp. 4831–4846, 2020.

[66] A. Zappone and E. Jorswieck, "Energy efficiency in wireless networks via fractional programming theory," *Found Trends in Commun. Inf. Theory*, vol. 11, no. 3–4, pp. 185–396, 2015.

[67] M. Soleymani, I. Santamaria, and P. J. Schreier, "Improper Gaussian signaling for the K -user MIMO interference channels with hardware impairments," *IEEE Trans. Veh. Technol.*, vol. 69, no. 10, pp. 11632–11645, 2020.

[68] G. R. Lanckriet and B. K. Sriperumbudur, "On the convergence of the concave-convex procedure," in *Proc. Adv. Neural Inf. Process. Syst.*, 2009, pp. 1759–1767.

[69] T. Lipp and S. Boyd, "Variations and extension of the convex-concave procedure," *Optim. Eng.*, vol. 17, no. 2, pp. 263–287, 2016.

- [70] Y. Xu, Y. Mao, O. Dizdar, and B. Clerckx, “Rate-splitting multiple access with finite blocklength for short-packet and low-latency downlink communications,” *IEEE Trans. Veh. Technol.*, 2022.
- [71] M. Shehab, H. Alves, E. A. Jorswieck, E. Dostì, and M. Latva-Aho, “Effective energy efficiency of ultrareliable low-latency communication,” *IEEE Internet Things J.*, vol. 8, no. 14, pp. 11 135–11 149, 2021.
- [72] M. Soleymani, I. Santamaria, and P. J. Schreier, “Distributed algorithms for spectral and energy-efficiency maximization of K-user interference channels,” *IEEE Access*, vol. 9, pp. 96 948–96 963, 2021.
- [73] X. Ou, X. Xie, H. Lu, H. Yang, and H. Tang, “Energy-efficient resource allocation for short packet transmission in MISO multicarrier NOMA,” *IEEE Trans. Veh. Technol.*, pp. 1–14, 2022.
- [74] G. Zhou, C. Pan, H. Ren, K. Wang, and A. Nallanathan, “A framework of robust transmission design for IRS-aided MISO communications with imperfect cascaded channels,” *IEEE Trans. Signal Process.*, vol. 68, pp. 5092–5106, 2020.
- [75] L. Wei, C. Huang, G. C. Alexandropoulos, C. Yuen, Z. Zhang, and M. Debbah, “Channel estimation for RIS-empowered multi-user MISO wireless communications,” *IEEE Trans. Commun.*, vol. 69, no. 6, pp. 4144–4157, 2021.
- [76] M. Soleymani, C. Lameiro, I. Santamaria, and P. J. Schreier, “Improper signaling for SISO two-user interference channels with additive asymmetric hardware distortion,” *IEEE Trans. Commun.*, vol. 67, no. 12, pp. 8624–8638, 2019.